Precambrian Research 233 (2013) 337–357

Contents lists available at SciVerse ScienceDirect

Precambrian Research

journal homepage: www.elsevier.com/locate/precamres

Episodic crustal growth in the southern segment of the Trans-North China Orogen across the Archean-Proterozoic boundary

Xiao-Long Huang[a,*], Simon A. Wilde[b], Jun-Wei Zhong[a,c]

[a] State Key Laboratory of Isotope Geochemistry, Guangzhou Institute of Geochemistry, Chinese Academy of Sciences, Guangzhou 510640, China
[b] Department of Applied Geology, Curtin University, PO Box U1987, Perth, Western Australia 6845, Australia
[c] Faculty of Land Resource Engineering, Kunming University of Science and Technology, Kunming 650093, China

ARTICLE INFO

Article history:
Received 17 April 2013
Received in revised form 23 May 2013
Accepted 23 May 2013
Available online 2 June 2013

Keywords:
TTG
Subduction
Early Paleoproterozoic
Late Archean
Columbia supercontinent
North China Craton

ABSTRACT

The Dengfeng and Taihua Complexes are well-exposed Neoarchean to Paleoproterozoic units in the southern segment of the Trans-North China Orogen (TNCO). Zircon U–Pb dating shows that the Dengfeng Complex records two episodes (2568 ± 11 Ma and 2306 ± 6 Ma) of tonalite–trondhjemite–granodiorite (TTG) magmatism. All of the TTG rocks are characterized by high SiO_2 (66.7–75.4 wt%), Na_2O (3.20–5.06 wt%) and relatively low MgO (0.40–1.78 wt%). The Late Neoarchean TTG gneisses have very low contents of HREE (Yb_N = 0.69–2.75) and Y (1.73–7.07 ppm), with moderate $[La/Yb]_N$ (24.1–53.8) and high Sr/Y (65.1–291.3) ratios. The Early Paleoproterozoic TTG gneisses have low contents of HREE (Yb_N = 2.93–6.37) and Y (6.7–11.0 ppm), with moderate $[La/Yb]_N$ (10.1–27.0) and Sr/Y (10.6–52.1) ratios. Both suites show pronounced negative Nb–Ta, P and Ti anomalies but positive Sr and Pb anomalies. The Late Neoarchean TTG gneisses all have similar bulk-rock Nd and zircon Hf model ages with mainly positive $\varepsilon_{Nd}(t)$, and are interpreted as resulting from the melting of dominantly juvenile thickened lower crust with residual garnet and amphibole. The Early Paleoproterozoic TTG gneisses have extremely variable $\varepsilon_{Nd}(t)$ (−6.23 to +4.23) and heterogeneous zircon $\varepsilon_{Hf}(t)$ (−3.3 to +3.1), which are also best interpreted as resulting from the partial melting of thickened lower crust with residual amphibole and garnet. The Taihua Complex in the Xiaoqinling area records three episodes of Early Paleoproterozoic TTG magmatism (2.48 Ga at Caotan, 2.31 Ga at Houjiacun and 2.16 Ga at Bayuan), younger than the Taihua Complex in the Lushan area (2.85–2.72 Ga). All rocks have relatively low contents of HREE (Yb_N = 1.03–8.32) and Y (2.84–24 ppm), with moderate $[La/Yb]_N$ (8.7–88.4) and Sr/Y (19.8–125.8) ratios, and show negative Ta–Nb and Ti anomalies and positive Sr and Pb anomalies. The Caotan gneisses at 2.48 Ga and the Houjiacun TTG gneisses at 2.31 Ga have low $Mg^{\#}$ (0.14–0.45), low Cr (<42 ppm) and Ni contents (1–21 ppm), with variable but overall positive $\varepsilon_{Nd}(t)$ and $\varepsilon_{Hf}(t)$ values, and were derived from the partial melting of thickened lower crust with residual garnet and amphibole. The younger Bayuan TTG gneisses at 2.16 Ga have low SiO_2 (57.11–64.89 wt%), high MgO (2.64–4.62 wt%), Cr (100–247 ppm) and Ni (32–80 ppm), with negative whole rock $\varepsilon_{Nd}(t)$ and zircon $\varepsilon_{Hf}(t)$ values, resulted from the partial melting of delaminated lower crust that interacted with peridotitic mantle.

The geochronology of the Dengfeng Complex (in the Dengfeng area) and the Taihua Complex (in the Lushan, Xiong'er and Xiaoqinling areas) reveals at least four magmatic episodes in the southern segment of the TNCO from the Late Mesoarchean to Early Paleoproterozoic (2.85–2.72 Ga, 2.57–2.48 Ga, 2.34–2.30 Ga and 2.20–2.07 Ga). The rocks of the two early episodes are dominantly of juvenile compositions with mostly positive whole rock $\varepsilon_{Nd}(t)$ and zircon $\varepsilon_{Hf}(t)$ values, suggesting two episodes of crustal growth formed in a subduction tectonic setting. The magmatic rocks of the third episode consist of both the juvenile and pre-existing crustal materials with variable whole rock $\varepsilon_{Nd}(t)$ and zircon $\varepsilon_{Hf}(t)$ values, which were generated in a subduction zone during the initial assembly of the NCC within the Columbia supercontinent cycle. The final episode of magmatism lacks juvenile materials with whole rock $\varepsilon_{Nd}(t)$ and zircon $\varepsilon_{Hf}(t)$ values being consistently negative. These may have resulted from the orogenic collapse. The episodic continental growth recorded in the southern segment of the TNCO was caused by subduction and consequent orogeny, consistent with global supercontinent cycles within the Late Archean and Early Paleoproterozoic.

* Corresponding author at: Guangzhou Institute of Geochemistry, Chinese Academy of Sciences, PO Box 1131, Guangzhou 510640, China. Tel.: +86 20 85290010; fax: +86 20 85291510.
E-mail address: xlhuang@gig.ac.cn (X.-L. Huang).

0301-9268/$ – see front matter © 2013 Elsevier B.V. All rights reserved.
http://dx.doi.org/10.1016/j.precamres.2013.05.016

1. Introduction

The North China Craton (NCC; Fig. 1a) is the oldest cratonic block in China (~3.8 Ga; Liu et al., 1992), with widespread Archean to Paleoproterozoic rocks (Fig. 1a) forming during several tectonic cycles (e.g., Zhao et al., 2005, 2012; Lu et al., 2008; Zhai et al., 2010; Zhao and Zhai, 2013). It is commonly recognized that the NCC resulted from amalgamation of several microblocks, but the timing and processes involved are still a subject of debate (e.g., Kusky and Li, 2003; Zhai et al., 2000, 2005, 2010; Zhao, 2001; Zhao et al., 2005, 2012; Zhao and Zhai, 2013), with several competing models proposed. Zhai et al. (2000, 2005, 2010) proposed that the NCC can be divided into several microblocks connected by greenstone belts and granites and were amalgamated at the end of the Neoarchean (~2.5 Ga). Zhao (2001) initially proposed that the NCC formed by amalgamation of the Eastern and Western Blocks along the Trans-North China Orogen (TNCO; Fig. 1a) at ~1.85. Later, Zhao et al. (2005) proposed that the Western Block formed by amalgamation of the Yinshan and Orodos Blocks along the Khondalite Belt at ~1.95 Ga (Zhao et al., 2003a, 2010; Zhao, 2009; Zhou et al., 2010), whereas the Eastern Block experienced a Paleoproterozoic rifting event forming the Jiao-Liao-Ji Belt at ~1.90 Ga (Li et al., 2004, 2006a,b; Luo et al., 2004; Zhou et al., 2008; Tam et al., 2011). However, Kusky and Li (2003) argued that the Eastern and Western Blocks amalgamated along a Central Orogenic Belt (COB) at ~2.5 Ga and the 1.9–1.8 Ga tectonothermal event was related to the collision along the northern margin of the NCC. To resolve these controversies, it is vital to determine the ages and petrogenesis of rocks in the TNCO that are considered to have resulted from the tectonic process that was operative at some time close to the Archean/Proterozoic transition.

Based on the geochronology and petrology of the metamorphic complexes (Fig. 1a) in the northern and central segments of the TNCO, Zhao et al. (2008a,b) proposed that the TNCO may represent a long-lived magmatic arc (>650 Ma). However, it still remains unknown whether or not the southern segment of the TNCO (Fig. 1a) also underwent such a long-lived subduction, though available data indicate that the Taihua and Dengfeng Complexes experienced a series of magmatic events from the Late Archean to Early Paleoproterozoic (Wan et al., 2006; Diwu et al., 2007, 2011; Liu et al., 2009, 2012a,b; Huang et al., 2010, 2012).

There are many published chronological and geochemical investigations on the Taihua Complex in the Xiong'er (Diwu et al., 2007; Huang et al., 2012) and Lushan (Wan et al., 2006; Liu et al., 2009; Xu et al., 2009; Huang et al., 2010) areas, but very few reliable geochronological and geochemical studies have been done on the Taihua Complex in the Xiaoqinling area (Fig. 1b) even though it is the largest outcrop of Precambrian basement in the southern segment of the TNCO. On the basis of Sm–Nd isochrons, depleted mantle Nd model ages, Ar–Ar dating, and single-grain zircon evaporation Pb–Pb ages, it has been suggested that the Taihua Complex in the Xiaoqinling area was comparable with other areas (BGMR, 1982; Qi, 1992; Zhou et al., 1998). However, in situ zircon U–Pb dates for the Taihua Complex in the Lushan and Xiong'er areas showed different crystallization ages (Diwu et al., 2007; Liu et al., 2009; Huang et al., 2010, 2012), and it is important to examine whether or not rocks in the Xiaoqinling area can be correlated with either of these areas.

Numerous chronological and geochemical investigations on the Dengfeng Complex have been carried out at Datasi, Huishansi, Lujiagou and Shipaihe (e.g., Li et al., 1987; Kröner et al., 1988; Wang et al., 2004; Wan et al., 2009; Diwu et al., 2011; Zhang et al., 2013), but no integrated dataset (i.e., major and trace elements, isotopes and geochronology) is available for rocks across the whole area. Thus, little is known about their petrogenesis and information that is relevant to crustal accretion and development of the NCC. Additionally, from the range of ages in the complex in different areas, it is unclear whether or not the southern segment of the TNCO shares a common crustal evolution.

In this study, we present integrated whole-rock geochemistry and Nd isotopes, and in situ zircon U–Pb ages and Hf isotopic data for TTG gneisses from the Taihua Complex in the Xiaoqinling area and for the Dengfeng Complex in the vicinity of Dengfeng City in order to determine the crystallization ages and investigate their petrogenetic processes. In combination with previous studies on the Taihua and Dengfeng Complexes, we outline the overall crustal evolution of the southern segment of the TNCO from the Late Archean to Early Paleoproterozoic, thus straddling the Archean/Proterozoic boundary and the period when crustal blocks were undergoing amalgamation.

2. Geological background

As mentioned above, the North China Craton can be divided into the Eastern and Western Blocks separated by the Paleoproterozoic Trans-North China Orogen (TNCO; Fig. 1a) (Zhao et al., 2000, 2001, 2002a), which was also referred to as "the Central Orogenic Belt" (e.g., Kusky and Li, 2003; Polat et al., 2005, 2006; Kusky, 2011). The Western Block can be subdivided into the Ordos Block in the south and the Yinshan Block in the north (Fig. 1a), which are considered to have amalgamated along the east–west-trending Khondalite Belt at ~1.95 Ga (e.g., Zhao et al., 2005; Xia et al., 2006a,b, 2008; Yin et al., 2009, 2011; Li et al., 2011; Wang et al., 2011). The Eastern Block can be further subdivided into the Longgang and Langrim Blocks separated by the Paleoproterozoic Jiao-Liao-Ji Belt (Fig. 1a; Li and Zhao, 2007; Luo et al., 2004; Tam et al., 2011). The Late Archean basement of the Eastern and Western Blocks is dominated by Neoarchean TTG gneiss domes surrounded by minor supracrustal rocks that underwent greenschist to granulite facies metamorphism at ~2.5 Ga (Zhao et al., 2005). The Archean rocks of the southern NCC include the Dengfeng and Taihua "Groups" (now referred to as the Dengfeng Complex and the Taihua Complex, respectively; Zhang et al., 1985). The Taihua Complex is exposed eastward from the Xiaoqinling to the Xiaoshan, Xiong'er, Lushan and Wuyang areas in the southern most segment of the TNCO (Fig. 1a).

The Taihua Complex in the Xiaoqinling area was traditionally regarded as a meta-volcanic sedimentary sequence, and was further subdivided into the Lower and Upper Taihua "Groups" according to rock types (Qi, 1992; Guan, 1996; Ding, 1996), similar to those in the Lushan and Xiong'er areas (Huang et al., 2010, 2012). The Upper Taihua "Group" consists of quartzite, metapelitic gneiss and schist, marble and iron formation, whereas the Lower Taihua "Group" consists of meta-basic volcanic rocks (amphibolite) and intermediate to felsic gneisses (biotite–plagioclase gneiss and plagioclase–amphibole gneiss), with minor granulites (Qi, 1992; Ding, 1996). There is evidence of widespread migmatization in the Lower Taihua "Group", and the amphibolite occurs as elongated enclaves in the gneisses, elongated parallel to the gneissic banding. The Taihua Complex in the Xiaoqinling area is unconformably covered by the Tietonggou Formation at Bayuan (Fig. 1b), which consists dominantly of Paleoproterozoic metamorphosed clastic rocks. Mesozoic granites intrude the Taihua Complex in this area and are abundant throughout the eastern and western parts (Fig. 1b).

The Dengfeng Complex is unconformably overlain by the Late Paleoproterozoic Songshan Group in the northeast and by the Early Mesoproterozoic Wufushan Group in the north (Fig. 1c). The Songshan Group is composed of low-grade metamorphic quartzite and schist with a strong fabric, whereas the Wufushan Group consists mainly of unmetamorphosed limestone, shale, siltstone, sandstone and conglomerate (Ma et al., 1975). The Dengfeng "Group" was

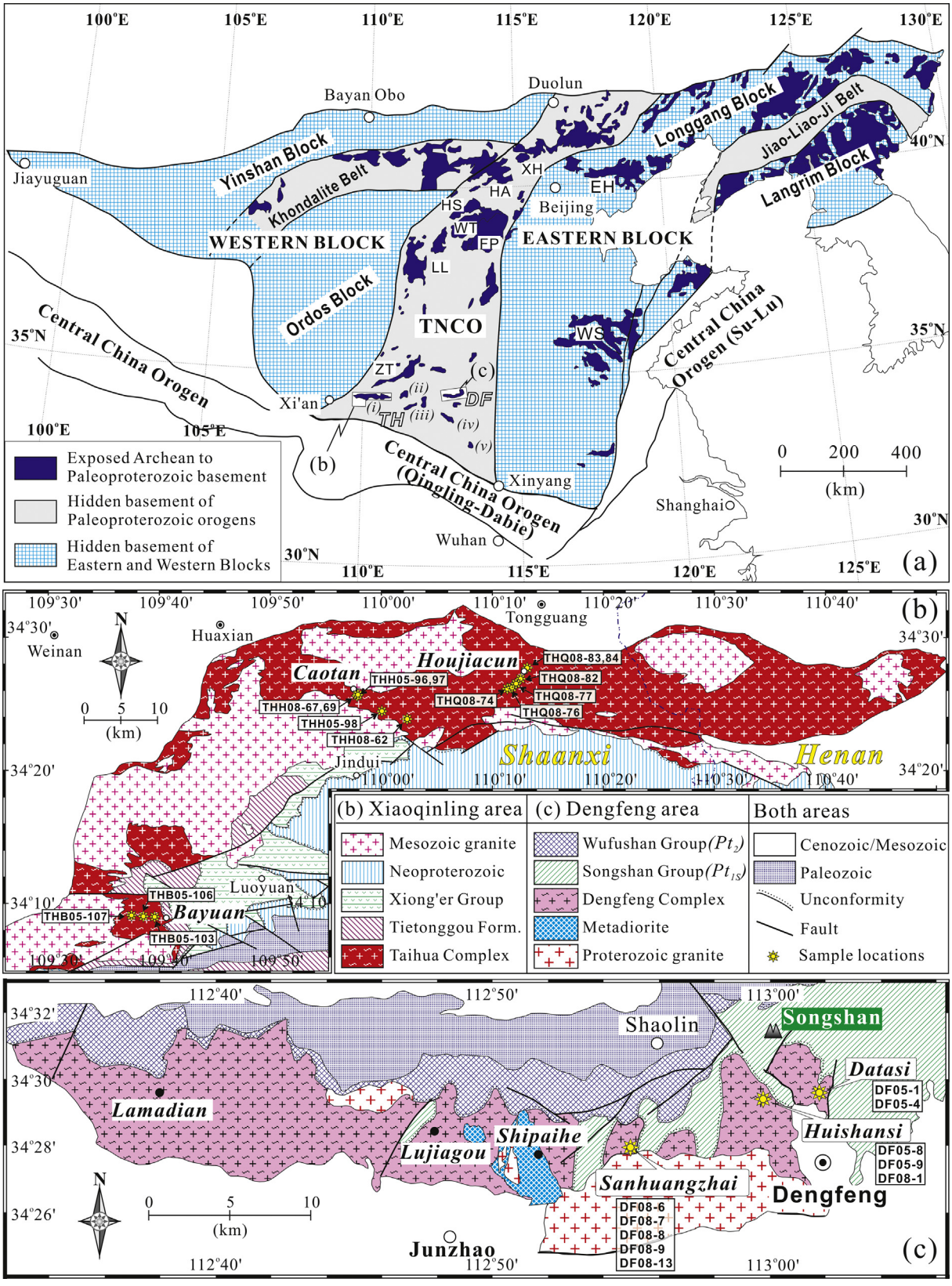

Fig. 1. (a) Tectonic framework of the North China Craton (NCC) showing the subdivision into Eastern Block, Western Block, Trans-North China Orogen (TNCO) and exposed Archean to Paleoproterozoic basement (after Zhao et al., 2005, 2012); the Taihua (TH) and the Dengfeng (DF) metamorphic complexes are located in the southern segment of the TNCO. The Taihua Complex includes: (i) Xiaoqinling; (ii) Xiaoshan; (iii) Xiong'er Mountain; (iv) Lushan; and (v) Wuyang. Abbreviations of other metamorphic complexes: Zhongtiaoshan (ZT), Wutaishan (WT), Fuping (FP), Lüliang (LL), Western Shandong (WS) and Eastern Hebei (EH); (b) geological map of the Xiaoqinling region, illustrating the distribution of the Taihua Complex and sample locations; modified after the Luonan and Weinan geological maps at 1:200,000 scale (BGMR, 1968); (c) geological map of the Dengfeng region, illustrating the distribution of the Dengfeng "Group" and sample locations; modified after the Linru and Xuchang geological maps of 1:200,000 scale (BGMR, 1965).

traditionally considered to represent a meta-volcano-sedimentary sequence exhibiting the essential features of a granite-greenstone terrane, with a volcano-sedimentary sequence intruded by early Na-rich granitoids and later K-rich granitic plutons (Zhang et al., 1985; Guo, 1988). The Na-rich granitic rocks are TTG that constitute the dominant component of the complex (~70% of the exposed rocks; Zhang et al., 1985; Guo, 1988). The later K-rich granitic rocks are less abundant and intruded the Na-rich granitic rocks (Guo, 1988). The Dengfeng Complex in the Shipaihe area also contains metadiorite that intruded into the lower part of the sequence, with both unconformably covered by the Songshan Group (Fig. 1c).

3. Samples and petrography

Samples of intermediate to felsic gneisses from the Taihua Complex in the Xiaoqinling area were collected from Houjiacun, Caotan and Bayuan (Fig. 1b). The gneisses are characterized by granoblastic textures, and have typical gneissic layering defined by variations in mineral proportions. According to the mineral assemblages, the gneisses can be classified as quartz diorite-tonalite gneiss (5–30% biotite, 5–40% amphibole, 30–65% plagioclase, 5–20% quartz), granite gneiss (5–15% biotite, 0–10% amphibole, 30–60% plagioclase, 5–30% K-feldspar and 20–30% quartz), and K-feldspar-rich granite gneiss (<5% biotite, <5% amphibole, 15–20% plagioclase, 40–45% K-feldspar and 30–35% quartz). Titanite, magnetite and apatite are common accessory minerals (<1%) in all gneisses. Sixteen fresh samples were selected for geochemical study. The samples from Bayuan are all tonalite gneiss, whereas the samples from Caotan are dominantly tonalite gneiss, with examples of granite gneiss and K-feldspar-rich granite gneiss, and the samples from Houjiacun are mainly tonalite gneiss, with some granite gneiss.

The gneiss samples from the Dengfeng Complex were collected from Datasi, Huishansi and Sanhuangzhai in the vicinity of Dengfeng City (Fig. 1c). The TTG gneisses from Huishansi and Datasi consist of plagioclase (45–65%), quartz (15–30%), biotite (10–25%), amphibole (<5%) and K-feldspar (<5%), and have a granoblastic texture with gneissosity defined by mineral variations. The tonalite and granite gneisses from Sanhuangzhai are layered and contain recrystallised quartz ribbons. The mineral assemblage is plagioclase (30–70%), quartz (20–40%), K-feldspar (5–40%), amphibole (<5%) and biotite (<5%). Titanite, magnetite, zircon and apatite are common accessory minerals (<1%) in all samples.

4. Analytical methods

Geochemical and Nd isotopic analyses were carried out at the Guangzhou Institute of Geochemistry, Chinese Academy of Sciences (GIG-CAS). Major element oxides were analyzed using a Rigaku RIX 2000 X-ray fluorescence spectrometer (XRF), and analytical uncertainties are mostly between 1% and 5% (Li et al., 2006a,b).

Trace elements were obtained by inductively coupled plasma mass spectrometry (ICP-MS), and detailed procedures are described by Li et al. (2006a,b). The USGS and Chinese National standards AGV-2, GSR-1, GSR-2, MRG-1, BCR-1, W-2 and G-2 were chosen for calibrating element concentrations of the analyzed samples. Analytical precision of REE and other incompatible elements is typically 1–5%.

Nd isotopic analyses were performed on a Micromass Isoprobe multi-collector ICP-MS (MC-ICP-MS), using analytical procedures described by Li et al. (2006a,b). REE were separated using cation exchange columns, and Nd fractions were further separated by HDEHP-coated Kef columns. The aqueous sample solution was taken up in 2% HNO_3 and introduced into the MC-ICP-MS using a Meinhard glass nebulizer with an uptake rate of 0.1 ml/min. The inlet system was cleaned for 5 min between analyses using high purity 5% HNO_3 followed by a blank solution of 2% HNO_3. Measured $^{143}Nd/^{144}Nd$ ratios were normalized to $^{146}Nd/^{144}Nd = 0.7219$. The reported $^{143}Nd/^{144}Nd$ ratios were adjusted to the Shin Etsu JNdi-1 standard of 0.512115. A long-term average $^{143}Nd/^{144}Nd$ of 0.512119 ± 13 (2σ; $n = 22$) for the Shin Etsu JNdi-1 standard was obtained during the period of this study.

Zircons were separated using conventional heavy liquid and magnetic techniques and purified by hand-picking under a binocular microscope. They were mounted together with a standard zircon (TEMORA) in epoxy resin. The mount was polished to expose the grain centers and then gold coated. The internal structure of the zircons was examined using cathodoluminescence (CL) prior to U–Pb isotopic analysis in order to identify suitable analytical sites. Zircon U–Pb analyses of samples DF05-9 (Huishansi), THH05-97 (Caotan) and THB05-103 (Bayuan) were performed using the Sensitive High-Resolution Ion Microprobe (SHRIMP II) at the Beijing SHRIMP Center (The Institute of Geology, Chinese Academy of Geological Sciences, Beijing); analytical procedures are similar to those described by Williams (1998). The intensity of the primary ^{2-}O ion beam was 4–6 nA. Primary beam size was ~30 μm, and each analytical site was rastered for 2–3 min prior to analysis. Five scans through the mass stations were made for each analysis. The standard TEMORA zircon ($^{206}Pb/^{207}Pb$ age of 417 Ma) was used for correction of inter-element fractionation and U, Th and Pb concentrations were determined relative to the standard Sri Lankan gem zircon SL13, which has a U concentration of 238 ppm and an age of 572 Ma. The Squid (ver. 1.02; Ludwig, 2001) and Isoplot (ver. 3.23) programs (Ludwig, 2003) were used for raw data reduction and age calculation, and common lead was corrected using the measured ^{204}Pb. Uncertainties reported in Supplemental Table 1 are all $\pm 1\sigma$, whereas the weighted mean ages quoted in the text ($^{207}Pb/^{206}Pb$ ages) are at the 95% confidence level.

Zircon U–Pb analyses of samples DF08-7 (Sanhuangzhai), THH08-62 (Caotan), and THQ08-76 and THQ08-82 (Houjiacun) were performed on the CAMECA ims-1280 ion microprobe at the Institute of Geology and Geophysics, Chinese Academy of Sciences (IGG-CAS) in Beijing, China. Analytical procedures are similar to those described by Li et al. (2009). U–Th–Pb isotopic ratios and absolute abundances were determined relative to the standard zircon 91500 (Wiedenbeck et al., 1995). Measured Pb isotopic compositions were corrected for common Pb using the measured ^{204}Pb. Data reduction was carried out using Isoplot (ver. 3.23) (Ludwig, 2003) and uncertainties on individual analyses in Supplemental Table 2 are reported at the 1σ level.

In situ zircon Hf isotopic analyses were carried out on the dated spots using a Neptune MC-ICPMS, equipped with a 193 nm laser, at the IGG-CAS. Spot sizes of 40 μm with a laser repetition rate of 8 Hz were used, with a signal intensity of ~5 V at ^{180}Hf mass with an energy density of 15 J/cm^2. The detailed analytical technique and data correction procedures are described in Wu et al. (2006). The mean β_{Yb} ($^{172}Yb/^{173}Yb$) value obtained from zircon was applied for the interference correction of ^{176}Yb and ^{176}Lu on ^{176}Hf (Wu et al., 2006; Xie et al., 2008). $^{176}Yb/^{172}Yb = 0.5886$ and $^{176}Lu/^{175}Lu = 0.02655$ were used for the elemental fractionation correction (Chu et al., 2002). Due to the extremely low $^{176}Lu/^{177}Hf$ in zircon (normally < 0.002 in the studied samples), the isobaric interference of ^{176}Lu on ^{176}Hf is negligible (Iizuka and Hirata, 2005). No relationship between $^{176}Yb/^{177}Hf$ and $^{176}Hf/^{177}Hf$ ratios was observed in the studied samples, indicating that the correction of ^{176}Yb interference on ^{176}Hf is precise for obtaining accurate $^{176}Hf/^{177}Hf$ values. During analysis of the samples, the zircon standard 91500 applied for the instrumental mass fractionation gave $^{176}Hf/^{177}Hf = 0.282292 \pm 14$ (2σ), which is identical within error to the $^{176}Hf/^{177}Hf$ ratio of 0.282284 ± 22 reported by Griffin et al. (2006). The uncertainties of

calibrated isotope ratios include those from the sample, standards, and reference values, which are given at $\pm 2\sigma$ in Supplemental Table 3.

5. Results

5.1. In situ zircon U–Pb geochronology

5.1.1. Dengfeng Complex: Huishansi granodioritic gneiss

Zircons from granodioritic gneiss sample DF05-9 (Huishansi) are all euhedral prismatic grains and CL images show well-developed oscillatory zoning (Fig. 2a), indicating a magmatic origin. The zircons contain moderate to high Th and U contents (108–560 ppm and 274–1486 ppm, respectively; Supplemental Table 1) with Th/U ratios of 0.29–0.62 (Supplemental Table 1). The data are strongly discordant but define an upper intercept age of 2568 ± 11 Ma (MSWD = 3.1; Fig. 2b), which is within error of Huishansi trondhjemite gneiss result (2553 ± 8 Ma) of Wan et al. (2009). Both results are taken to define the crystallization age of the gneiss protolith, slightly older than that of the Datasi tonalite gneiss (2531 ± 9 Ma; Wan et al., 2009).

5.1.2. Dengfeng Complex: Sanhuangzhai tonalite gneiss

Zircons from tonalite gneiss sample DF08-7 (Sanhuangzhai) are mostly euhedral and elongate to stubby. CL images of most zircons show oscillatory zoning in the cores, but some rims are darker and free of zoning (Fig. 2c). All analyses have high Th/U ratios of 0.36–1.54 with moderate to high Th and U contents (100–803 ppm and 120–1301 ppm, respectively; Supplemental Table 2). The U–Pb results show a tight grouping of concordant to near concordant apparent $^{207}Pb/^{206}Pb$ ages, with a weighted mean value of 2306 ± 6 Ma (Fig. 2d), which is interpreted as the crystallization age of the Sanhuangzhai tonalite gneiss. The analyses of Spots 7.1, 9.1 and 11.1 on the rim or transitional area to the core (Fig. 2d) have younger apparent $^{207}Pb/^{206}Pb$ ages (2185 ± 7 Ma to 2260 ± 8 Ma; Supplemental Table 2), indicating recrystallization during a later metamorphic event.

5.1.3. Taihua Complex: Bayuan tonalite gneiss

Zircons from tonalite gneiss sample THB05-103 (Bayuan) are mostly stubby and CL images show well-developed oscillatory zoning (Fig. 3a). Thirteen zircons were analyzed and they have moderate to high Th and U contents (219–533 ppm and 401–1050 ppm, respectively) with high Th/U ratios of 0.45–1.08 (Supplemental Table 1). Two analyses on cores (Spots 1.1 and 5.1; Fig. 3a) give older apparent $^{207}Pb/^{206}Pb$ ages (2324 ± 27 Ma and 2278 ± 6 Ma, respectively). However nine U–Pb results are concentrated on concordia and define a weighted mean $^{207}Pb/^{206}Pb$ age of 2164 ± 16 Ma (MSWD = 1.8; Fig. 3b). This is interpreted as the crystallization age of the Bayuan tonalite gneiss.

5.1.4. Taihua Complex: Caotan gneisses

Tonalite gneiss sample THH05-97 and granite gneiss sample THH08-62 were selected for zircon U–Pb dating by SHRIMP and CAMECA, respectively. The zircons are mostly euhedral prismatic grains (Fig. 3c and e). CL images of zircons from samples THH05-97 and THH08-62 show well-developed oscillatory zoning in the core with rims generally free of zoning (Fig. 3c and e). Some zircons from sample THH08-62 show a patchy structure with very weak oscillatory zoning or turbid structures indicative of recrystallization (Fig. 3e).

Fifteen zircons from tonalite gneiss sample THH05-97 were analyzed on the oscillatory zoned cores, and three were also analyzed on the rims (Supplemental Table 1). The zircons contain variable Th and U contents (84–1289 ppm and 11–2374 ppm, respectively) with variable Th/U ratios of 0.09–1.90 (Supplemental Table 1). Three analyses on the rims have low Th/U ratios of 0.09–0.14, whereas most of the core analyses have high Th/U ratios (>0.31, except for Spots 4.1 and 9.1; Supplemental Table 1). All analyses contain low common lead with $f_{206} < 0.27\%$ (Supplemental Table 1). The apparent $^{207}Pb/^{206}Pb$ ages of the zircon cores are concentrated between either 2547–2555 Ma or 2470–2502 Ma, corresponding to weighted mean $^{207}Pb/^{206}Pb$ ages of 2552 ± 4 Ma and 2477 ± 8 Ma, respectively (Fig. 3d; Supplemental Table 1). The younger weighted mean $^{207}Pb/^{206}Pb$ age (2477 ± 8 Ma) is interpreted as the crystallization age of the Caotan tonalite gneiss, whereas the older weighted mean $^{207}Pb/^{206}Pb$ age (2552 ± 4 Ma) is interpreted as age of the inherited zircons. Spot 8.2 on the rim gives the youngest apparent $^{207}Pb/^{206}Pb$ age of 1912 ± 12 Ma, similar to its apparent $^{206}Pb/^{238}U$ age of 1891 ± 19 Ma, which is taken to approximate the time of metamorphism.

Twenty-one zircons from granite gneiss sample THH08-62 were analyzed on the cores, whereas eight analyses (Spots 3, 5, 6, 7, 9, 16, 19 and 21) were made on sites without zoning and all have low Th/U ratios (mostly < 0.12, except for Spot 21; Supplemental Table 2). These latter are metamorphic domains with young apparent $^{207}Pb/^{206}Pb$ ages ranging from 1759 ± 2 Ma to 1936 ± 9 Ma, and define an upper intercept age of 1918 ± 17 Ma (Fig. 3f) that is identical within error to the metamorphic age of 1912 ± 12 Ma obtained from tonalite gneiss sample THH05-97 (Fig. 3d). Eight analyses on sites with oscillatory zoning (Spots 1, 2, 10, 11, 12, 13, 14, and 17) have older apparent $^{207}Pb/^{206}Pb$ ages ranging from 2429 ± 6 Ma to 2505 ± 5 Ma (Supplemental Table 2), with a weighted mean age of 2477 ± 28 Ma (Fig. 3f), interpreted as the crystallization age of the Caotan granite gneiss. This is identical to the age of the Caotan tonalite gneiss (2477 ± 8 Ma; Fig. 3d).

5.1.5. Taihua Complex: Houjiacun gneisses

Tonalite gneiss sample THQ08-76 and granite gneiss sample THQ08-82 were selected for zircon U–Pb dating by CAMECA ims-1280.

The zircons from sample THQ08-76 are mostly euhedral with either oscillatory or sector zoning (Fig. 3g). Twenty-seven analyses have variable Th and U contents (56–1428 ppm and 94–1421 ppm, respectively) with high Th/U ratios of 0.41–1.01 (Supplemental Table 2). Except for Spot 13, the U–Pb results form a coherent cluster and yield a concordia age of 2311 ± 1 Ma (MSWD = 1.1) and a weighted mean $^{207}Pb/^{206}Pb$ age of 2311 ± 3 Ma (MSWD = 1.2; Fig. 3h), which is interpreted as the crystallization age of the Houjiacun tonalite gneiss.

The zircons from sample THQ08-82 are mainly subhedral with oscillatory zoned cores and structureless rims, although a few grains have an oscillatory zoned mantle with both core and rim free of zoning (Fig. 3i). Eight analyses on the cores with oscillatory zoning (Spots 2, 4, 6, 7, 8, 9, 10 and 11) have high Th/U ratios of 0.52–0.90 with moderate Th and U contents (145–568 ppm and 206–639 ppm, respectively; Supplemental Table 2). They have similar apparent $^{207}Pb/^{206}Pb$ ages from 2297 ± 7 Ma to 2315 ± 6 Ma (Supplemental Table 2), corresponding to a weighted mean age of 2307 ± 5 Ma (MSWD = 1.2) (Fig. 3j), which is interpreted as the crystallization age of the Houjiacun granite gneiss. This is within error of the crystallization age of the Houjiacun tonalite gneiss (2311 ± 1 Ma; Fig. 3h). The analyses on the structureless cores (Spots 12 and 14; Fig. 3i) have high Th/U ratios (0.58 and 0.99; respectively). The analyses on the rims (Spots 13 and 15; Fig. 3i) have lower Th/U ratios (0.03 and 0.28; respectively). Site 13 is entirely within a structureless rim domain and the apparent $^{207}Pb/^{206}Pb$ age of 1862 ± 6 Ma is taken as the minimum estimate of the time of metamorphism.

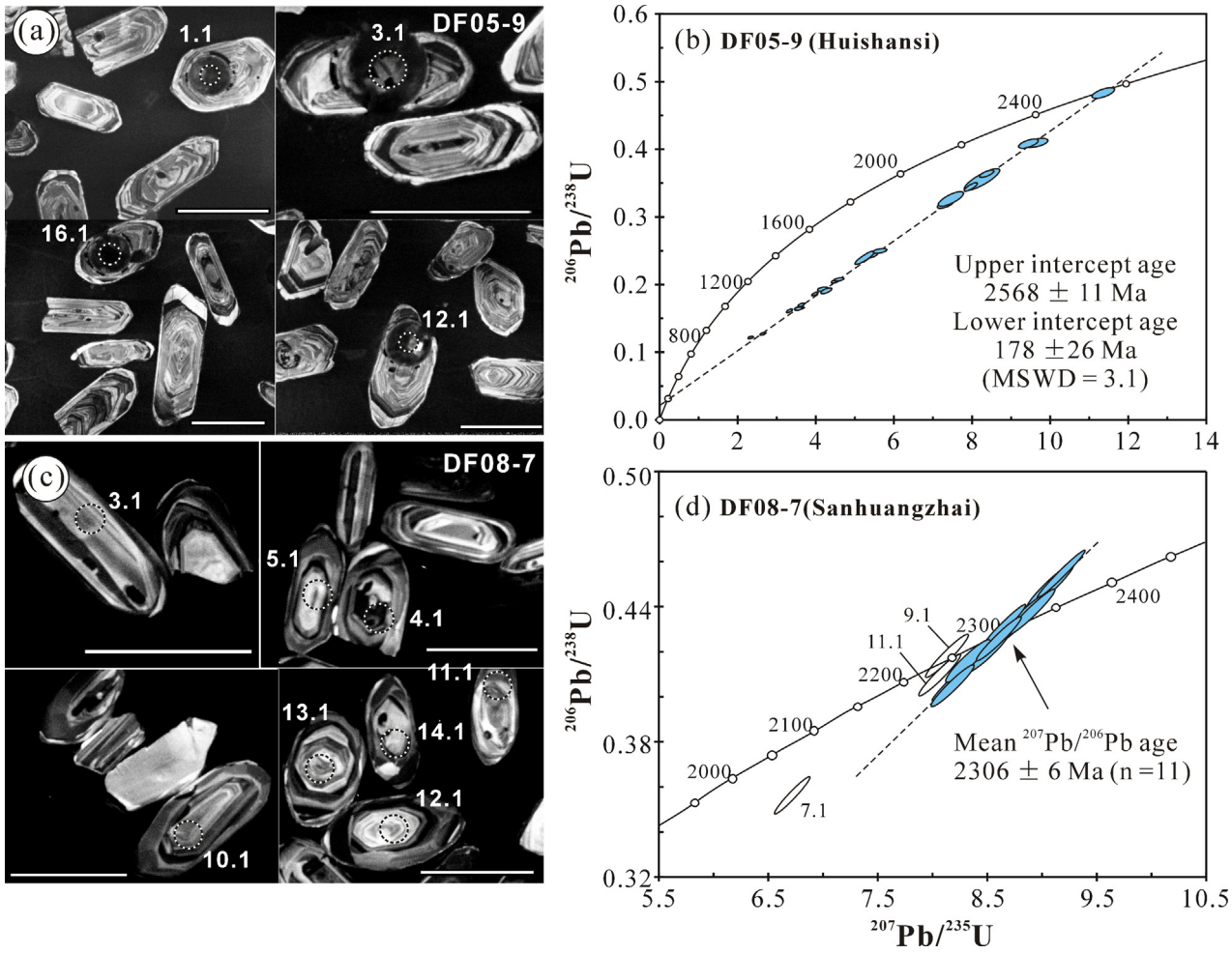

Fig. 2. CL images of zircons and concordia diagrams of zircon SIMS U–Pb geochronology of the Dengfeng Complex. (a and b) Granodioritic gneiss sample DF05-9 from Huishansi; (c and d) tonalitic gneiss sample DF08-7 from Sanhuangzhai. The dotted circles indicate U–Pb dating sites (30 μm diameter) and corresponding laser ablation sites for in situ zircon Hf isotopic analyses (40–50 μm diameter); the scale bar is 100 μm.

5.2. LA-MC-ICPMS zircon Lu–Hf isotope data

Most of zircons selected for Lu–Hf analyses were previously dated by SHRIMP or CAMECA ims-1280 on the same sites (Supplemental Table 3). The initial Hf isotope ratios were calculated both at the mean crystallization age (t) and $^{207}Pb/^{206}Pb$ age ($t_{7/6}$) determined for that site (Supplemental Table 3). The single-stage Hf model ages ($T_{DM\text{-}Hf}$) refer to extraction from a depleted mantle (Supplemental Table 3; Fig. 4), whereas the "crustal" model ages ($T_{DM\text{-}Hf}^{C}$) are calculated by assuming the parental magma was produced from average continental crust ($^{176}Lu/^{177}Hf = 0.015$) that was originally derived from the depleted mantle (Griffin et al., 2004).

5.2.1. The Dengfeng Complex

Zircons from granodiorite gneiss sample DF05-9 have similar $^{176}Hf/^{177}Hf$ ratios (0.281213–0.281328) and variable $\varepsilon_{Hf}(t_{7/6})$ values (−2.4 to +4.5) that are mostly positive (Fig. 4a; Supplemental Table 3). The single-stage Hf model ages ($T_{DM\text{-}Hf}$) range from 2666 Ma to 2832 Ma, whereas the two-stage "crustal" model ages ($T_{DM\text{-}Hf}^{C}$) are older and range from 2723 Ma to 2984 Ma (Supplemental Table 3).

Zircons from tonalite gneiss sample DF08-7 have $^{176}Hf/^{177}Hf$ ratios of 0.281251–0.281437 with variable $\varepsilon_{Hf}(t_{7/6})$ values (−3.3 to +3.1) (Fig. 4a), single-stage Hf model ages of 2537–2791 Ma and two-stage "crustal" model ages of 2675–3077 Ma (Supplemental Table 3).

Zircon $\varepsilon_{Hf}(t_{7/6})$ values of both DF05-9 and DF08-7, calculated using their $^{207}Pb/^{206}Pb$ ages, plot below the depleted mantle evolution curve (Griffin et al., 2000) (Fig. 4a), with zircon $\varepsilon_{Hf}(t_{7/6})$ values of granodiorite gneiss sample DF08-7 generally more negative than those of tonalite gneiss sample DF05-9 (Supplemental Table 3; Fig. 4a). Furthermore, two-stage "crustal" model ages ($T_{DM\text{-}Hf}^{C}$) for zircons from sample DF08-7 vary over a wider range than those from sample DF05-9 (Supplemental Table 3). The "crustal" model ages would be 2.72–2.98 Ga (DF05-9) and 2.68–3.08 Ga (DF08-7), respectively, using the average continental crustal $^{176}Lu/^{177}Hf$ value (0.015) (Supplemental Table 3).

5.2.2. The Taihua Complex in the Xiaoqinling area

5.2.2.1. The Bayuan gneiss. Zircons from tonalite gneiss sample THB05-103 have $^{176}Hf/^{177}Hf$ ratios of 0.281228–0.281400 with negative $\varepsilon_{Hf}(t_{7/6})$ values of −6.0 to −2.2 (Supplemental Table 3; Fig. 4b). Single-stage Hf model ages (2607–2819 Ma; Supplemental Table 3) and "crustal" model ages (2861–3217 Ma; Supplemental Table 3) are all much older than the crystallization age of 2168 ± 13 Ma.

5.2.2.2. The Caotan gneisses. Zircons from tonalite gneiss sample THH05-97 have variable $\varepsilon_{Hf}(t_{7/6})$ values (−9.3 to +3.4) that are mostly positive (Fig. 4b; Supplemental Table 3), corresponding to single-stage Hf model ages of 2576–2832 Ma and "crustal" model ages of 2636–3043 Ma (Supplemental Table 3). Zircons from

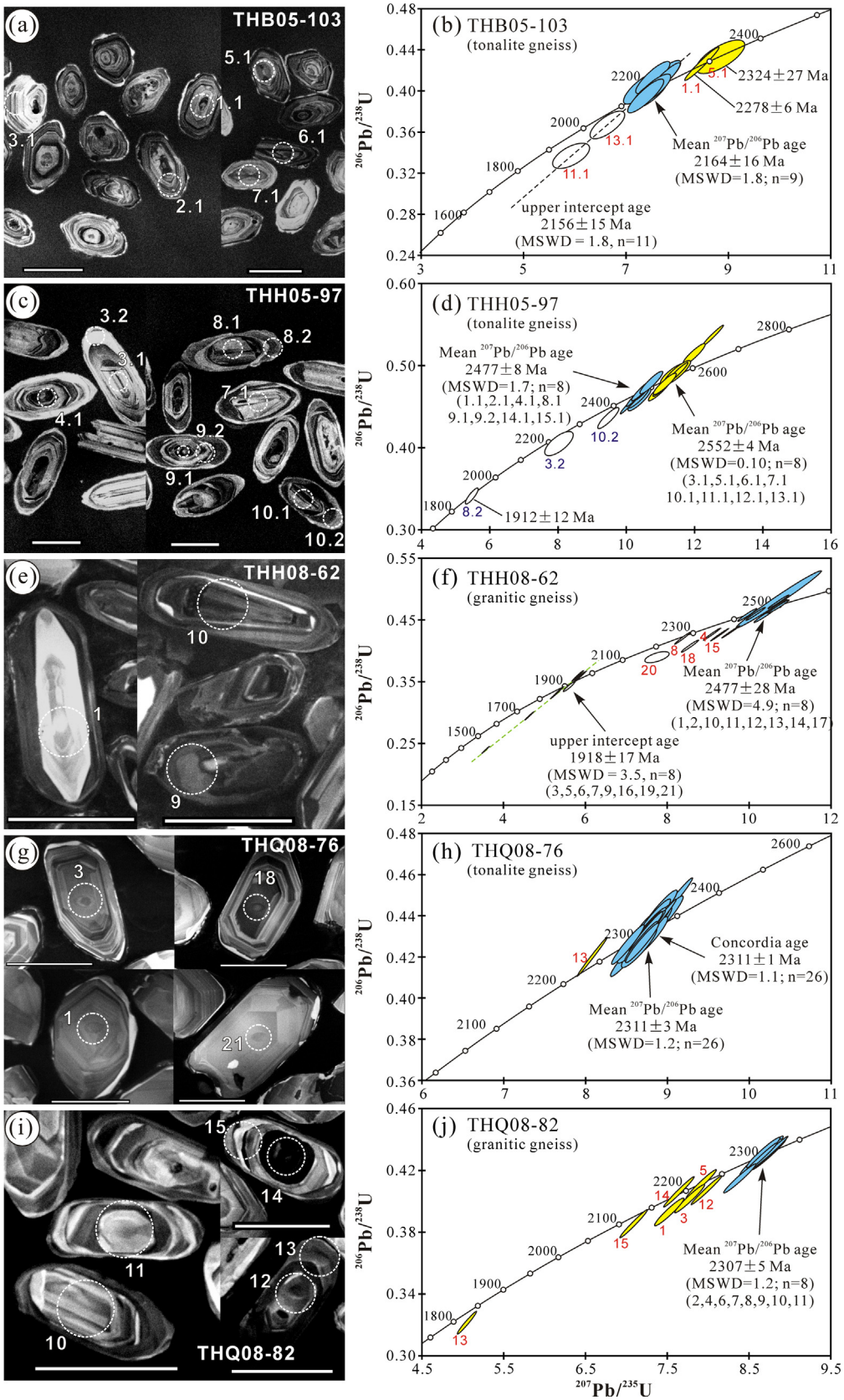

Fig. 3. CL images of zircons and concordia diagrams of zircon SIMS U–Pb geochronology of the Taihua Complex in the Xiaoqinling area. (a and b) Tonalite gneiss sample THB05-103 from Bayuan; (c and d) tonalite gneiss sample THH05-97 from Caotan; (e and f) granite gneiss sample THH08-62 from Caotan; (g and h) tonalite gneiss sample THQ08-76 from Houjiacun; (i and j) granite gneiss sample THQ08-82 from Houjiacun. The dotted circles indicate dating sites (30 μm diameter) and corresponding laser ablation sites for in situ zircon Hf isotopic analyses (40–50 μm diameter); the scale bar is 100 μm.

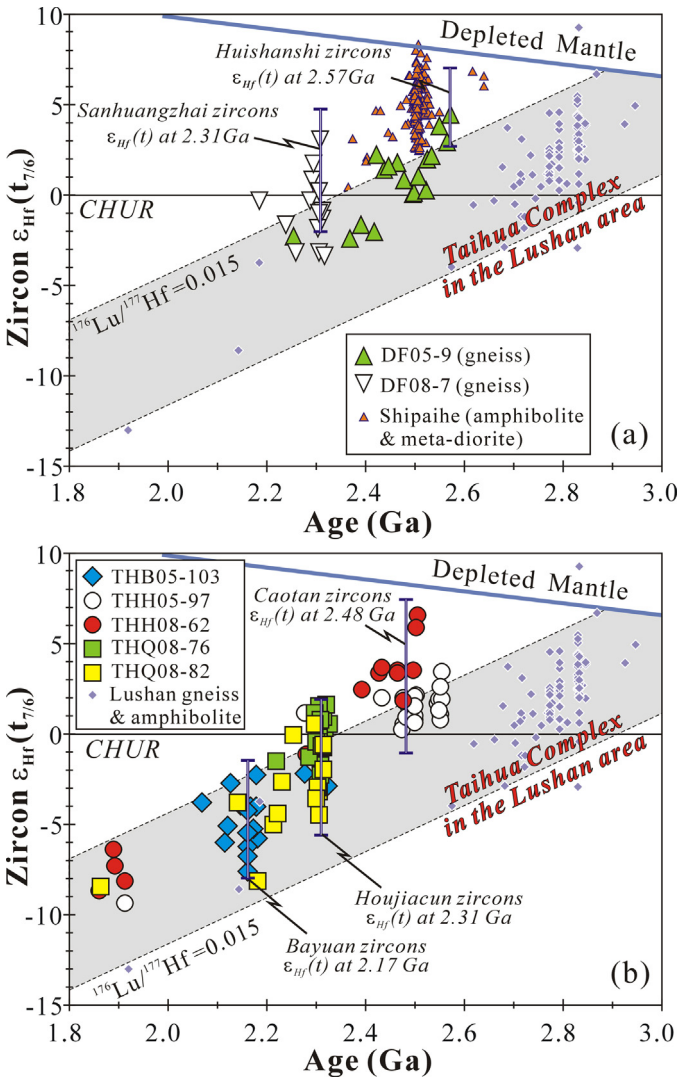

Fig. 4. Hf isotope evolution diagram and frequency distribution of single-stage primitive mantle Hf model ages for zircons from TTG gneisses of the Dengfeng Complex (a) and the Taihua Complex in the Xiaoqinling area (b). Zircon data for the TTG gneisses from the Taihua Complex in the Lushan area (Huang et al., 2010) are shown for comparison. Data plotted based on individual apparent $^{207}Pb/^{206}Pb$ ages ($t_{7/6}$); line bar shows the range of data based on the crystallization age (t) of rock; the evolution of depleted mantle (DM) is drawn by using a present-day $^{176}Hf/^{177}Hf = 0.28325$ and $^{176}Lu/^{177}Hf = 0.0384$ (Griffin et al., 2000).

granite gneiss sample THH08-62 have variable, but mostly positive, $\varepsilon_{Hf}(t_{7/6})$ values (−11.1 to +6.6) (Fig. 4b; Supplemental Table 3), and both $T_{DM\text{-}Hf}$ (2533–2730 Ma) and $T_{DM\text{-}Hf}^{C}$ (2564–2879 Ma) are younger than those from sample THH05-97 (Supplemental Table 3). The youngest zircon $T_{DM\text{-}Hf}$ (2533 ± 23 Ma; Supplemental Table 3) of the Caotan gneisses is slightly older than its crystallization age of 2477 ± 8 Ma.

5.2.2.3. The Houjiacun gneisses. The $^{176}Hf/^{177}Hf$ ratios of zircons from tonalite gneiss sample THQ08-76 vary over a relatively narrow range of 0.281302–0.281395, corresponding to $\varepsilon_{Hf}(t_{7/6})$ values of −2.3 to +1.6 that are mostly negative (Supplemental Table 3; Fig. 4b). The single-stage Hf model ages ($T_{DM\text{-}Hf}$) and "crustal" model ages ($T_{DM\text{-}HF}^{C}$) all vary in narrow ranges of 2592–2758 Ma and 2757–2995 Ma, respectively (Supplemental Table 3), and are much older than the crystallization age of 2311 ± 1 Ma. The zircons from granite gneiss sample THQ08-82 have variable $^{176}Hf/^{177}Hf$ ratios of 0.281250–0.281374, corresponding to variable $\varepsilon_{Hf}(t_{7/6})$ values (−8.5 to +0.5) that are mostly negative (Fig. 4b), with old single-stage Hf model ages and "crustal" model ages of 2585–2886 Ma and 2752–3185 Ma, respectively (Supplemental Table 3). The youngest $T_{DM\text{-}Hf}$ and $T_{DM\text{-}HF}^{C}$ model ages of granite gneiss sample THQ08-82 (2585 ± 22 Ma and 2752 ± 22 Ma, respectively; Supplemental Table 3) are similar to those of tonalite gneiss sample THQ08-76 (2592 ± 21 Ma and 2757 ± 21 Ma, respectively; Supplemental Table 3).

Zircon $\varepsilon_{Hf}(t_{7/6})$ values of the Taihua gneisses in the Xiaoqinling area calculated using the apparent $^{207}Pb/^{206}Pb$ ages are all lower than the evolution curve of the depleted mantle (Griffin et al., 2000) (Fig. 4b). Zircons from the Bayuan sample (THB05-103) have a similar Lu–Hf isotope protolith to those of the Taihua Complex in the Lushan area (Liu et al., 2009; Huang et al., 2010) using the crustal $^{176}Lu/^{177}Hf$ value of 0.015 (Fig. 4b). However, the zircons from the Houjiacun (THQ08-76 and THQ08-82) and Caotan samples (THH05-97 and THH08-62) show overall more positive $\varepsilon_{Hf}(t)$ values and younger "crustal" model ages than those of the Taihua Complex in the Lushan area, indicating an overall younger protolith (Fig. 4b).

5.3. Major and trace elements

The gneisses from Huishansi, Datasi and Sanhuangzhai in the Dengfeng Complex have high SiO_2 and Na_2O, but relatively low MgO, Fe_2O_3, TiO_2 and CaO (Table 1). The Bayuan gneisses of the Taihua Complex in the Xiaoqinling area have low SiO_2 and Na_2O, and high CaO, MgO, Fe_2O_3, Cr and Ni with $Mg^{\#}$ of 0.44–0.56 (Table 1). The Caotan and Houjiacun gneisses of the Taihua Complex in the Xiaoqinling area contain variable SiO_2, CaO, Na_2O, K_2O, MgO and Fe_2O_3, and low TiO_2, Cr and Ni with low $Mg^{\#}$ of 0.14–0.45 (Table 1). The Houjiacun gneisses show overall lower SiO_2, but higher MgO and CaO and TiO_2 than the Caotan gneisses (Fig. 5a–c). The gneiss samples of the Dengfeng and Taihua Complexes show a general trend of decreasing MgO, CaO and TiO_2 with increasing SiO_2 (Fig. 5a–c).

In the Ab-Or-An diagram (Barker and Arth, 1976), the samples from the Dengfeng Complex range from tonalite, trondhjemite, and granodiorite to granite, although most plot in the fields of tonalite and trondhjemite (Fig. 6). The Caotan gneisses plot in the fields of tonalite, granodiorite and trondhjemite, except for two high-SiO_2 samples (THH05-96 and THH08-62) plotting in the field of granite (Fig. 6). The Houjiacun and Bayuan gneisses plot in the fields of tonalite and granodiorite, and have a higher proportion of An than the Caotan gneisses (Fig. 6).

All Dengfeng gneisses have LREE-enriched and HREE-depleted patterns (Fig. 7a). The Huishansi and Datasi gneisses have low HREE (Yb_N = 0.69–2.75) and Y (1.73–7.07 ppm), with moderate $[La/Yb]_N$ (24.1–53.8) and high Sr/Y (65.1–291.3) (Table 1). Datasi gneisses have weak negative or weak positive Eu anomalies (Eu/Eu^* = 0.95–1.13; Table 1; Fig. 7a), but sample DF05-1 shows a distinctively positive Eu anomaly (Eu/Eu^* = 1.39; Table 1; Fig. 7a). The Sanhuangzhai gneisses have higher HREE (Yb_N = 2.93–6.37) and Y (6.7–11.0 ppm), with moderate $[La/Yb]_N$ (10.1–27.0), Sr/Y (10.6–52.1) and weak negative Eu anomalies (0.72–0.99; Table 1; Fig. 7a). On the primitive mantle-normalized spidergrams, all Dengfeng gneisses are characterized by pronounced negative Nb, Ta and Ti anomalies and positive Sr and Pb anomalies (Fig. 7b).

The gneisses from Houjiacun and Bayuan in the Taihua Complex have fractionated REE patterns ($[La/Yb]_N$ = 7.2–30.6; Table 1; Fig. 7c) with weak negative or positive Eu anomalies (Eu/Eu^* = 0.84–1.15; Table 1; Fig. 7c), and show negative Ta, Nb and Ti anomalies (Fig. 7d). Samples from Bayuan also have positive Pb and Sr anomalies (Fig. 7d), and contain lower HREE than those from Houjiacun (Fig. 7c). The gneisses from Caotan all have very low HREE contents (Yb_N = 1.03–2.63) and Y (2.84–7.40 ppm) and weak negative or positive Eu anomalies (Eu/Eu^* = 0.85–1.15;

Table 1
Major (wt%) and trace element (ppm) data for gneisses in the Dengfeng and Taihua Complexes.

Sample	DF05-1	DF05-4	DF05-8	DF05-9	DF08-1	DF08-6	DF08-7	DF08-8	DF08-9
Location	DTS	DTS	HSS	HSS	HSS	SHZ	SHZ	SHZ	SHZ
SiO_2	66.67	66.74	69.03	68.70	69.74	69.95	68.13	75.31	68.02
TiO_2	0.31	0.38	0.31	0.29	0.30	0.29	0.33	0.09	0.33
Al_2O_3	17.61	15.89	17.50	16.38	16.31	15.75	16.07	14.45	16.00
Fe_2O_3	2.88	4.31	2.29	2.83	2.33	2.24	2.96	0.78	2.95
MnO	0.03	0.05	0.03	0.03	0.03	0.04	0.04	0.02	0.04
MgO	1.30	1.78	0.70	1.19	1.08	1.29	1.33	0.40	1.34
CaO	3.43	3.83	1.02	2.01	2.74	2.16	3.42	1.83	3.56
Na_2O	4.28	3.51	5.06	3.20	4.36	4.73	4.38	5.06	4.26
K_2O	2.04	2.22	2.41	2.96	2.05	2.08	1.93	1.59	1.80
P_2O_5	0.12	0.12	0.07	0.08	0.09	0.08	0.10	0.03	0.09
LOI	0.70	1.04	1.41	1.56	1.26	1.47	1.46	0.67	1.41
Total	99.36	99.86	99.84	99.21	100.30	100.06	100.14	100.25	99.80
$Mg^{\#}$	0.47	0.45	0.38	0.45	0.48	0.53	0.47	0.51	0.47
Sc	1.66	4.51	0.91	2.53	3.47	5.59	6.42	2.89	6.27
Ti	1942	2312	1928	1751	1608	1442	1699	507	1720
V	28	43	21	28	30	30	34	10	34
Cr	6	32	1	8	8	2	4	2	4
Co	7	11	3	5	47	49	31	38	37
Ni	9	17	1	4	9	8	10	3	11
Cu	5.70	6.97	20.5	5.32	1.55	1.96	16.6	28.3	18.7
Zn	43.8	45.7	13.8	29.1	41	30.2	44.0	13.9	48.4
Ga	17.0	16.4	17.9	18.1	17.9	16.6	16.7	14.5	17.2
Ge	0.64	0.97	0.57	0.82	0.75	1.02	0.94	0.84	0.93
Rb	62	68	59	92	59	94	72	40	69
Sr	504	460	489	379	504	294	358	228	356
Y	1.73	7.07	3.78	2.76	3.30	11.0	6.87	6.69	8.46
Ba	846	1130	906	890	643	714	799	756	688
Zr	130	146	191	119	126	125	150	66.7	148
Hf	3.01	3.75	4.28	2.76	3.13	3.70	3.86	2.64	3.83
Nb	3.00	5.15	2.97	3.04	3.16	5.03	4.59	4.31	4.57
Ta	0.18	0.43	0.34	0.29	0.40	0.94	0.57	0.94	0.52
Pb	9.07	11.2	4.73	5.52	8.89	10.7	10.7	11.8	10.7
Th	1.02	7.88	4.76	4.89	5.58	8.23	8.04	5.57	7.55
U	0.51	1.43	0.63	0.81	0.66	1.78	1.46	1.61	1.31
La	9.13	24.2	26.2	19.6	20.3	23.7	30.1	11.2	29.1
Ce	15.4	44.9	53.1	32.8	32.2	39.9	49.8	19.9	49.6
Pr	1.62	5.01	5.74	3.83	3.42	3.84	4.76	2.08	4.86
Nd	5.19	17.0	19.2	12.6	11.4	12.6	15.5	7.28	16.0
Sm	0.81	2.71	2.62	1.90	1.57	2.00	2.25	1.42	2.49
Eu	0.49	0.76	0.74	0.67	0.52	0.61	0.71	0.38	0.68
Gd	0.71	2.33	1.62	1.14	1.17	2.04	2.13	1.42	2.30
Tb	0.076	0.27	0.17	0.14	0.14	0.32	0.27	0.23	0.33
Dy	0.37	1.35	0.72	0.54	0.67	1.97	1.45	1.35	1.75
Ho	0.068	0.26	0.13	0.11	0.13	0.43	0.28	0.28	0.35
Er	0.18	0.66	0.36	0.26	0.32	1.30	0.78	0.78	1.01
Tm	0.026	0.10	0.055	0.036	0.046	0.22	0.12	0.11	0.16
Yb	0.17	0.68	0.33	0.25	0.30	1.58	0.75	0.73	1.19
Lu	0.025	0.11	0.053	0.038	0.048	0.26	0.12	0.11	0.19
Eu/Eu*	1.39	0.95	1.01	1.13	1.06	0.96	0.99	0.89	0.92
$[La/Yb]_N$	36.3	24.1	53.8	53.2	45.8	10.1	27.0	10.4	16.5
Sr/Y	291.3	65.1	129.5	137.0	152.8	26.6	52.1	34.0	42.0
Dy/Yb	2.18	1.99	2.18	2.16	2.23	1.25	1.93	1.85	1.47
Rb/Sr	0.12	0.15	0.12	0.24	0.12	0.32	0.20	0.18	0.19

Sample	DF08-13	THH05-96	THH05-97	THH05-98	THH08-62	THH08-67	THH08-69	THQ08-74	THQ08-76
Location	SHZ	CT	CT	CT	CT	CT	CT	HJC	HJC
SiO_2	75.35	73.57	67.44	61.35	73.01	68.47	68.24	58.46	61.70
TiO_2	0.11	0.15	0.44	0.54	0.22	0.41	0.32	0.63	0.60
Al_2O_3	13.32	13.99	15.21	17.56	14.31	15.53	13.71	16.81	17.28
Fe_2O_3	0.96	1.58	4.59	5.45	1.57	3.26	5.30	7.62	5.74
MnO	0.02	0.02	0.05	0.08	0.02	0.03	0.05	0.11	0.07
MgO	0.50	0.13	1.16	2.01	0.47	1.15	1.99	3.08	1.97
CaO	0.56	0.83	3.31	4.82	1.77	2.89	2.03	5.57	4.92
Na_2O	3.80	3.19	4.69	4.63	3.21	4.60	4.86	3.89	3.46
K_2O	4.22	5.96	2.57	2.47	4.72	2.84	2.42	2.43	2.06
P_2O_5	0.03	0.02	0.10	0.13	0.05	0.11	0.07	0.19	0.16
LOI	0.83	0.29	0.33	0.58	0.54	0.61	0.52	1.24	1.57
Total	99.68	99.75	99.90	99.62	99.90	99.90	99.51	100.02	99.53
$Mg^{\#}$	0.51	0.14	0.33	0.42	0.37	0.41	0.43	0.45	0.40
Sc	2.44	0.72	5.33	7.76	2.01	4.89	4.70	16.4	17.0
Ti	595	854	2848	3247	1221	2092	1685	3387	3265
V	11	9	39	59	20	28	33	120	54
Cr	2		18	26	2	15	10	12	15
Co	18	2	8	13	37	25	32	29	28

Table 1 (*continued*)

Sample	DF08-13	THH05-96	THH05-97	THH05-98	THH08-62	THH08-67	THH08-69	THQ08-74	THQ08-76
Location	SHZ	CT	CT	CT	CT	CT	CT	HJC	HJC
Ni	3	1	13	21	3	11	11	6	7
Cu	16.5	4.37	15.1	9.55	4.78	2.83	1.80	2.33	2.61
Zn	14.0	10.7	41.7	62.4	21.8	25.3	32.7	65.8	61.9
Ga	12.1	17.0	18.5	19.7	17.9	18.5	14.1	17.6	19.3
Ge	0.99	0.71	1.15	1.03	0.95	0.83	0.89	1.20	1.12
Rb	101	182	98	120	185	95	88	112	61
Sr	96.0	377	372	833	174	540	425	489	441
Y	9.06	3.68	7.40	6.62	2.84	6.83	7.23	15.3	24.0
Ba	1073	989	648	732	685	973	669	727	930
Zr	109	91.2	163	96.1	187	107	107	93.6	197
Hf	3.23	2.70	3.76	2.30	5.39	2.55	2.46	2.10	4.49
Nb	4.38	6.89	6.38	4.83	6.07	6.42	4.38	5.26	9.92
Ta	0.36	0.26	0.21	0.37	0.37	0.36	0.29	0.36	0.65
Pb	20.4	60.2	83.7	83.7	12.1	16.6	43.8	5.21	9.88
Th	28.0	15.6	5.16	7.07	18.6	11.7	4.73	3.98	7.32
U	2.95	1.82	0.28	1.16	1.10	0.36	0.49	0.54	0.98
La	34.6	20.5	27.9	23.4	32.4	64.0	27.5	24.5	43.8
Ce	54.4	37.3	47.1	42.1	62.8	110	49.9	50.4	88.7
Pr	4.85	3.96	5.53	4.35	6.11	11.0	5.09	5.81	10.1
Nd	15.4	12.8	18.0	15.0	19.7	34.3	17.4	22.2	39.0
Sm	2.50	2.03	3.04	2.45	2.83	4.11	2.59	3.81	6.83
Eu	0.44	0.68	0.92	0.96	0.64	0.90	0.73	1.07	1.42
Gd	2.67	1.43	2.43	1.90	2.23	3.29	2.16	3.35	5.90
Tb	0.36	0.15	0.29	0.24	0.20	0.32	0.26	0.49	0.81
Dy	1.94	0.77	1.37	1.21	0.72	1.38	1.29	2.67	4.28
Ho	0.36	0.13	0.26	0.24	0.11	0.24	0.26	0.56	0.84
Er	0.98	0.36	0.67	0.59	0.26	0.62	0.67	1.51	2.22
Tm	0.14	0.054	0.095	0.089	0.036	0.079	0.097	0.22	0.32
Yb	0.93	0.34	0.56	0.58	0.26	0.49	0.65	1.47	2.06
Lu	0.15	0.055	0.081	0.090	0.046	0.074	0.10	0.22	0.30
Eu/Eu*	0.72	1.07	1.00	1.15	0.87	0.85	0.96	0.95	0.82
$[La/Yb]_N$	25.0	40.4	33.7	27.2	85.9	88.4	28.4	11.2	14.3
Sr/Y	10.6	102.4	50.4	125.8	61.2	79.1	58.8	32.0	18.3
Dy/Yb	2.09	2.26	2.46	2.07	2.82	2.81	1.97	1.81	2.08
Rb/Sr	1.05	0.48	0.26	0.14	1.06	0.18	0.21	0.23	0.14

Sample	THQ08-77	THQ08-82	THQ08-83	THQ08-84	THB05-103	THB05-106	THB05-107
Location	HJC	HJC	HJC	HJC	BY	BY	BY
SiO_2	60.93	68.89	57.68	58.32	64.33	58.63	57.11
TiO_2	0.82	0.52	0.66	0.70	0.42	0.58	0.64
Al_2O_3	16.80	14.45	17.23	17.37	15.12	17.22	18.06
Fe_2O_3	6.25	4.53	7.86	7.87	6.67	7.34	7.60
MnO	0.08	0.06	0.12	0.13	0.09	0.10	0.10
MgO	2.58	1.02	2.97	2.67	2.64	4.62	3.94
CaO	3.73	2.72	6.25	6.56	4.64	5.59	6.17
Na_2O	3.88	3.21	4.23	4.50	2.13	2.94	2.96
K_2O	3.77	3.87	1.72	1.37	2.75	1.98	2.25
P_2O_5	0.24	0.12	0.16	0.19	0.09	0.18	0.19
LOI	0.69	0.26	0.73	0.68	0.79	0.63	0.90
Total	99.76	99.65	99.63	100.37	99.66	99.80	99.92
$Mg^{\#}$	0.45	0.31	0.43	0.40	0.44	0.56	0.51
Sc	13.8	10.9	21.6	20.7	14.1	11.1	15.4
Ti	4388	2845	3671	3931	2493	3497	3901
V	60	28	99	88	75	82	81
Cr	21	10	42	26	100	247	122
Co	23	31	25	38	17	20	24
Ni	7	5	12	11	32	80	58
Cu	9.00	6.47	3.58	4.59	23.6	10.8	33.1
Zn	78.3	60.6	89.1	75.2	52.4	73.0	69.2
Ga	19.4	17.0	19.8	18.9	17.2	20.4	21.3
Ge	1.08	1.12	1.34	1.20	1.47	1.44	1.33
Rb	133	96	70	34	113	128	93
Sr	407	323	391	510	325	638	555
Y	15.7	16.3	19.6	16.1	10.6	9.71	10.0
Ba	977	1763	392	484	591	676	879
Zr	205	268	167	119	140	115	154
Hf	4.84	6.63	3.86	2.73	3.49	2.64	3.39
Nb	8.69	8.71	8.09	7.17	7.33	7.30	8.05
Ta	0.60	0.45	0.54	0.63	0.64	0.49	0.54
Pb	11.9	16.1	6.04	7.55	16.0	15.9	20.5
Th	8.86	10.9	4.89	6.17	10.8	1.11	1.59
U	1.07	0.71	0.60	0.56	0.95	1.14	1.15
La	44.8	49.6	25.1	26.5	37.0	15.4	15.8
Ce	86.8	96.8	57.4	55.7	67.8	33.1	33.2
Pr	9.29	10.6	7.12	6.52	7.28	4.50	4.20

Table 1 (*continued*)

Sample	THQ08-77	THQ08-82	THQ08-83	THQ08-84	THB05-103	THB05-106	THB05-107
Location	HJC	HJC	HJC	HJC	BY	BY	BY
Nd	33.1	38.1	28.5	25.9	23.0	18.6	16.7
Sm	4.96	6.19	5.19	4.61	3.47	3.82	3.17
Eu	1.36	1.36	1.33	1.45	0.87	1.40	1.28
Gd	4.20	5.33	4.45	3.93	2.71	3.07	2.60
Tb	0.53	0.68	0.63	0.53	0.36	0.40	0.37
Dy	2.78	3.39	3.49	2.83	1.89	1.93	1.86
Ho	0.57	0.60	0.72	0.56	0.37	0.35	0.37
Er	1.55	1.47	1.94	1.51	1.04	0.94	0.97
Tm	0.22	0.18	0.29	0.21	0.17	0.14	0.14
Yb	1.48	1.09	1.96	1.43	1.07	0.85	1.01
Lu	0.24	0.16	0.30	0.22	0.17	0.13	0.14
Eu/Eu*	0.94	0.84	0.91	1.01	0.91	1.10	1.15
$[La/Yb]_N$	20.5	30.6	8.7	12.5	23.4	12.2	10.6
Sr/Y	26.0	19.8	19.9	31.7	30.7	65.7	55.3
Dy/Yb	1.88	3.10	1.78	1.98	1.78	2.27	1.84
Rb/Sr	0.33	0.30	0.18	0.07	0.35	0.20	0.17

Sample locations: (1) Datasi (DTS), Huishansi (HSS) and Sanhuangzhai (SHZ) in the Dengfeng Complex; (2) Caotan (CT), Houjiacun (HJC) and Bayuan (BY) in the Taihua Complex.

Table 1; Fig. 7c), with moderate to high $[La/Yb]_N$ (27.2–88.4) and Sr/Y (50.4–125.8) (Table 1). The Caotan samples are characterized by pronounced negative Nb, Ta and Ti anomalies and positive Sr and Pb anomalies, except for one high-SiO_2 sample (THH08-62) having no Sr and Pb anomalies (Fig. 7d).

All gneiss samples from the Dengfeng Complex plot in the field of adakite and high Al-TTG on the $[La/Yb]_N$ versus Yb_N and Sr/Y versus Y diagrams (Fig. 8). They are typical TTGs, with high SiO_2, high Na_2O and low ferromagnesian contents (Table 1; Fig. 5) (Martin et al., 2005). Overall, the Sanhuangzhai TTG gneisses have lower $[La/Yb]_N$ and Sr/Y ratios but higher Yb_N and Y than the Datasi and Huishansi TTG gneisses (Fig. 8). The Caotan and Bayuan gneiss samples all plot in the fields of adakite and high Al-TTG, and the Houjiacun gneisses mostly plot in the overlap fields of TTG and island arc magmatic rocks because of relatively high heavy REE and Y contents. The Caotan gneisses are typical TTGs with high SiO_2 and Na_2O, and low ferromagnesian contents (Table 1) (Martin et al., 2005). The Bayuan tonalite gneisses show similarities with the Archean sanukitoid suite, with low SiO_2 (57.11–64.33 wt%; Table 1) and high MgO, Sr, Ba, Cr and Ni contents (Table 1), and high $Mg^{\#}$ values (up to 0.56; Table 1). However, the Bayuan tonalite gneisses are not sanukitoids that are restricted to the Late Archean and always have higher MgO (>6 wt%) and $Mg^{\#}$ (>0.60) with lower SiO_2 (<60 wt%) (Martin et al., 2005).

5.4. Whole rock Nd isotopes

The Huishansi and Datasi TTG gneisses in the Dengfeng Complex all have positive $\varepsilon_{Nd}(t)$ values (+0.23 to +1.63), whereas the Sanhuangzhai TTG gneisses have variable $\varepsilon_{Nd}(t)$ of −6.23 to +4.23 (Table 2; Fig. 9). The Huishansi and Datasi TTG gneisses have similar single-stage depleted mantle model ages (T_{DM} = 2.73–2.83 Ga; Table 2) and two-stage model ages (T_{DM2} = 2.79–2.91 Ga; Table 2), whereas the Sanhuangzhai TTG gneisses show variable T_{DM} and T_{DM2} model ages in the range of 2.35–3.20 Ga (Table 2).

The Bayuan TTG gneisses have negative $\varepsilon_{Nd}(t)$ (−3.85 to −2.33) with Nd model ages (T_{DM} = 2.74–2.82 Ga; T_{DM2} = 2.78–2.90 Ga; Table 2) much older than the crystallization age of 2.17 Ga. The Caotan TTG gneisses have overall positive $\varepsilon_{Nd}(t)$ values of −0.07 to +2.85 (Table 2) with Nd model ages (T_{DM} = 2.60–2.78 Ga; T_{DM2} = 2.62–2.86 Ga; Table 2) slightly older than the crystallization age of 2.48 Ga. The Houjiacun TTG gneisses have variable $\varepsilon_{Nd}(t)$ of −1.32 to +2.22 (Table 2; Fig. 9) with young Nd model ages (T_{DM} = 2.51–2.75 Ga; T_{DM2} = 2.53–2.82 Ga; Table 2). Overall, the Taihua TTG gneisses in the Xiaoqinling area have younger Nd model ages (T_{DM} = 2.51–2.82 Ga; Table 2) than the Taihua Complex in the Lushan area (T_{DM} = 2.84–3.11 Ga; Huang et al., 2010).

6. Discussion

6.1. Petrogenesis

The high Sr/Y and La/Yb characteristic of the adakitic TTGs could result from melting of a high Sr/Y source (Moyen, 2009), but there is no evidence of any pre-existing high Sr/Y and La/Yb sources in the Dengfeng and Xiaoqinling areas. TTGs might represent partial melts of hydrous mafic rocks at pressures high enough to stabilize garnet ± amphibole, thus producing tonalitic melts with a characteristic signature of high La/Yb and Sr/Y ratios (e.g., Drummond and Defant, 1990; Smithies, 2000; Martin et al., 2005; Condie, 2005). Subducting ocean crust under eclogite facies conditions (Defant and Drummond, 1990; Kay et al., 1993; Martin, 1999; Martin et al., 2005), thickened lower crust (Smithies, 2000; Condie, 2005) or delaminated lower crust (Zegers and van Keken, 2001; Bédard, 2006) would be the potential source for TTGs. Partial melts of the subducting ocean crust and delaminated lower crust would interact with peridotitic mantle during ascent, resulting in high MgO, Cr and Ni contents (e.g., Rapp et al., 1999; Smithies, 2000; Martin et al., 2005; Wang et al., 2006), which would be one of the principal characteristics distinguishing them from partial melts of thickened lower crust.

6.1.1. Petrogenesis of the Dengfeng TTG gneisses

All the Neoarchean Dengfeng TTG gneisses have relatively constant and low Dy/Yb ratios, which are distinctly different from the Lushan TTG (Huang et al., 2010). Amphibole has a high K_D for HREEs, but even higher for middle REEs (e.g., Dy). Unlike amphibole, garnet has a progressive increasing K_D for REEs with increasing atomic number. Thus partial melting with a dominant residual phase of garnet will effectively raise the Dy/Yb ratios in the melt while a residual phase rich in amphibole will induce lower Dy/Yb ratios. Relatively invariable Dy/Yb of the Neoarchean Dengfeng TTG gneisses indicates that the high Sr/Y and La/Yb ratios could be attributed to fractionation of amphibole and garnet at relatively high pressures and partial melting with residual amphibole and garnet (e.g., PM-2 and FC-2 in Fig. 10). Even though high in SiO_2, the Paleoproterozoic Sanhuangzhai TTG gneisses have relatively high Y and HREE contents but low Sr/Y, La/Yb and Dy/Yb ratios, suggesting a low degree of partial melting, with the residue dominated by amphibole (e.g., PM-1 in Fig. 10). Additionally, variable Dy/Yb ratios

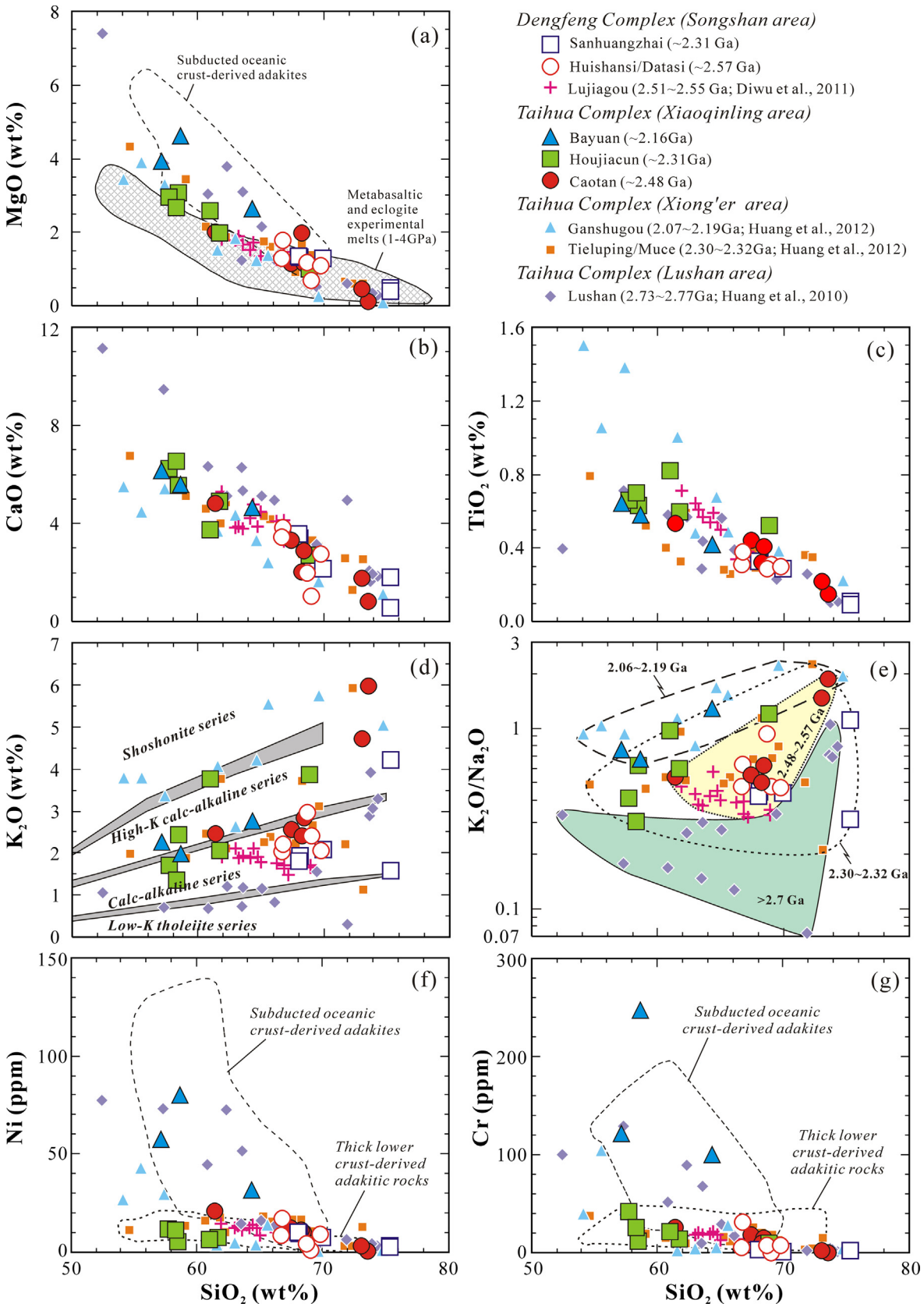

Fig. 5. Diagrams of (a) MgO, (b) CaO, (c) TiO_2, (d) K_2O, (e) K_2O/Na_2O, (f) Ni and (g) Cr versus SiO_2 for the TTG gneisses of the Dengfeng and Taihua Complexes. Fields of adakites in (a, f and g) are after the compilation of Wang et al. (2006). Large symbols – data from Table 1; small symbols – data from the literature (Huang et al., 2010, 2012; Diwu et al., 2011).

Table 2
Nd isotope compositions for gneisses in the Dengfeng and Taihua Complexes.

Samples	$^{147}Sm/^{144}Nd$[a]	$^{143}Nd/^{144}Nd$ ($\pm2\sigma$)	$(^{143}Nd/^{144}Nd)_i$	$\varepsilon_{Nd}(t)$[b]	$f_{Sm/Nd}$[c]	T_{DM} (Ga)[d]	T_{DM2} (Ga)[e]
Bayuan (Taihua)							
THB05-103	0.0913	0.510943 ± 8	0.509643	−3.85	−0.54	2.74	2.90
THB05-106	0.1241	0.511486 ± 6	0.509721	−2.33	−0.37	2.82	2.78
Caotan (Taihua)							
THH05-97	0.1020	0.511105 ± 7	0.509437	0.30	−0.48	2.78	2.83
THH05-98	0.0989	0.511184 ± 6	0.509567	2.85	−0.50	2.60	2.62
THH08-62	0.0868	0.510838 ± 12	0.509418	−0.07	−0.56	2.77	2.86
Houjiacun (Taihua)							
THQ08-74	0.1037	0.511336 ± 7	0.509757	2.22	−0.47	2.51	2.53
THQ08-76	0.1077	0.511302 ± 9	0.509663	0.37	−0.45	2.65	2.68
THQ08-77	0.0907	0.511047 ± 8	0.509666	0.44	−0.54	2.60	2.68
THQ08-82	0.0983	0.511072 ± 8	0.509576	−1.32	−0.50	2.73	2.82
THQ08-83	0.1103	0.511333 ± 7	0.509654	0.20	−0.44	2.67	2.70
Datasi-Huishansi (Dengfeng)							
DF05-1	0.0944	0.510943 ± 8	0.509343	0.31	−0.52	2.81	2.87
DF05-4	0.0964	0.510995 ± 8	0.509387	0.62	−0.51	2.79	2.84
DF05-8	0.0827	0.510790 ± 7	0.509390	1.63	−0.58	2.73	2.79
DF05-9	0.0913	0.510865 ± 8	0.509318	0.23	−0.54	2.83	2.91
Sanhuangzhai (Dengfeng)							
DF08-7	0.0876	0.510667 ± 7	0.509339	−6.23	−0.55	2.99	3.20
DF08-8	0.1181	0.511130 ± 7	0.509340	−6.21	−0.40	3.20	3.20
DF08-9	0.0941	0.511160 ± 7	0.509734	1.52	−0.52	2.53	2.58
DF08-13	0.0978	0.511354 ± 7	0.509872	4.23	−0.50	2.35	2.37

[a] Calculated by using whole-rock Sm and Nd contents listed in Table 1.
[b] $\varepsilon_{Nd}(t) = [(^{143}Nd/^{144}Nd)_S/(^{143}Nd/^{144}Nd)_{CHUR} - 1] \times 10{,}000$; t = 2.17 Ga (Bayuan), 2.31 Ga (Houjiacun), 2.48 Ga (Caotan); 2.57 Ga (Huishansi and Datasi), 2.31 Ga (Sanhuangzhai).
[c] $f_{Sm/Nd} = [(^{147}Sm/^{144}Nd)_S/(^{147}Sm/^{144}Nd)_{CHUR}] - 1$ (Shirey and Hanson, 1986).
[d] $T_{DM} = \ln\{[(^{143}Nd/^{144}Nd)_s - (^{143}Nd/^{144}Nd)_{DM}]/[(^{143}Sm/^{144}Nd)_s - (^{147}Sm/^{144}Nd)_{DM}]\}/\lambda$ (DePaolo, 1981).
[e] $T_{DM2} = T_{DM1} - (T_{DM1} - t)((f_{cc} - f_S)/(f_{cc} - f_{DM}))$ (Keto and Jacobsen, 1987); where S = sample, f_{cc}, f_S and f_{DM} are $f_{Sm/Nd}$ values of the average continental crust, the sample and the depleted mantle, respectively. In the calculation, $(^{143}Nd/^{144}Nd)_{CHUR}$ = 0.512638, $(^{147}Sm/^{144}Nd)_{CHUR}$ = 0.1967, $(^{143}Nd/^{144}Nd)_{DM}$ = 0.51315, $(^{147}Sm/^{144}Nd)_{DM}$ = 0.2136, f_{cc} = −0.4, f_{DM} = 0.08592.

of the Sanhuangzhai TTG gneisses can be attributed to fractionation of amphibole and garnet (e.g., FC-1 in Fig. 10).

Amphibole fractionation is commonly accompanied by plagioclase removal in natural systems, and the relatively low Eu/Eu* in the Paleoproterozoic Sanhuangzhai TTG gneisses indicates fractional crystallization of plagioclase. The net effect of amphibole and plagioclase fractionation is to increase La/Yb, and decrease Dy/Yb, accompanied by either a moderate increase or decrease in Sr/Y (Moyen, 2009), which might be a reasonable explanation why the Sanhuangzhai TTG gneisses have low and variable Dy/Yb ratios with moderate Sr/Y and La/Yb ratios. However, some Neoarchean Dengfeng TTG gneisses have high Sr/Y ratios, which are incompatible with low La/Yb ratios. Such TTG gneisses, with correspondingly high positive Eu anomalies (Table 1), are most likely the result of plagioclase accumulation (Fig. 10). In general, the Sr/Y and La/Yb ratios are similar to modern adakites, while the Neoarchean TTGs are less correlated (Moyen, 2009). As mentioned above, plagioclase fractionation or accumulation would change the Sr/Y ratios but have less effect on the La/Yb ratios, which might be one reason for the decoupling between Sr/Y and La/Yb in the Archean TTGs.

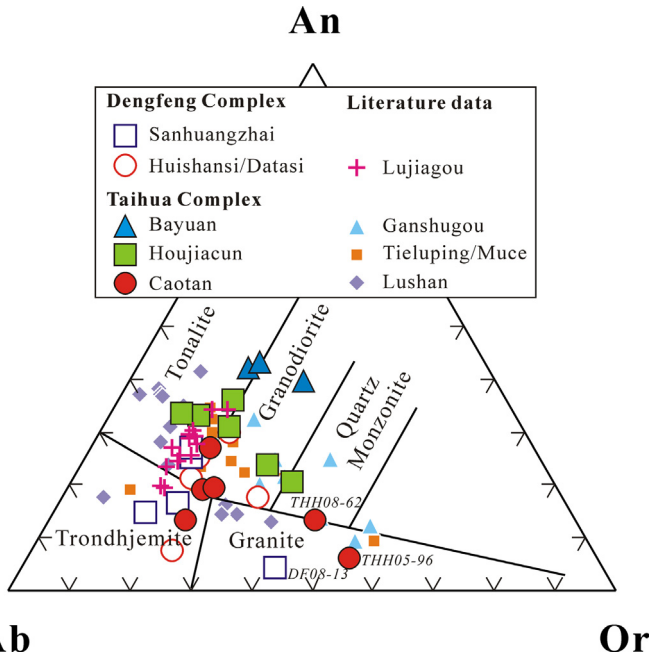

Fig. 6. Ab-Or-An classification diagram (Barker and Arth, 1976) for the TTG gneisses of the Dengfeng and Taihua Complexes. Large symbols – data from Table 1; small symbols – data from the literature (Huang et al., 2010, 2012; Diwu et al., 2011).

As most zircon $\varepsilon_{Hf}(t_{7/6})$ values for the Neoarchean TTG gneisses in the Dengfeng Complex plot distinctly below the depleted mantle line (Fig. 4a), pre-existing crustal material was involved in their genesis. The inherited zircons (2.60–2.95 Ga) in the Neoarchean TTG gneisses and felsic metavolcanics (Kröner et al., 1988; Wan et al., 2009) from the Dengfeng Complex indicate the presence of an earlier continental crust. Such early crust would be an appropriate source for the Neoarchean Dengfeng TTGs. On the other hand, because the Neoarchean TTG gneisses have positive $\varepsilon_{Nd}(t)$ values (Table 2) and mainly positive zircon $\varepsilon_{Hf}(t_{7/6})$ values (Supplemental Table 3; Fig. 4a), juvenile components are also present in their source. The Paleoproterozoic Sanhuangzhai TTG gneisses have relatively old zircon Hf "crustal" model ages of 2.68–3.08 Ga and two-stage Nd model ages (oldest T_{DM2} = 3.20 Ma). Some negative whole-rock $\varepsilon_{Nd}(t)$ and mainly negative zircon $\varepsilon_{Hf}(t_{7/6})$ values in the Sanhuangzhai TTG gneisses indicate that the source included pre-existing crustal materials, whereas the positive whole-rock $\varepsilon_{Nd}(t)$ and variable zircon $\varepsilon_{Hf}(t_{7/6})$ values of some samples require the participation of juvenile materials. Therefore, petrogenesis of the Dengfeng TTG gneisses requires the participation of both juvenile components and pre-existing crustal material, indicating Late Neoarchean to Early Paleoproterozoic crustal growth in the southern North China Craton.

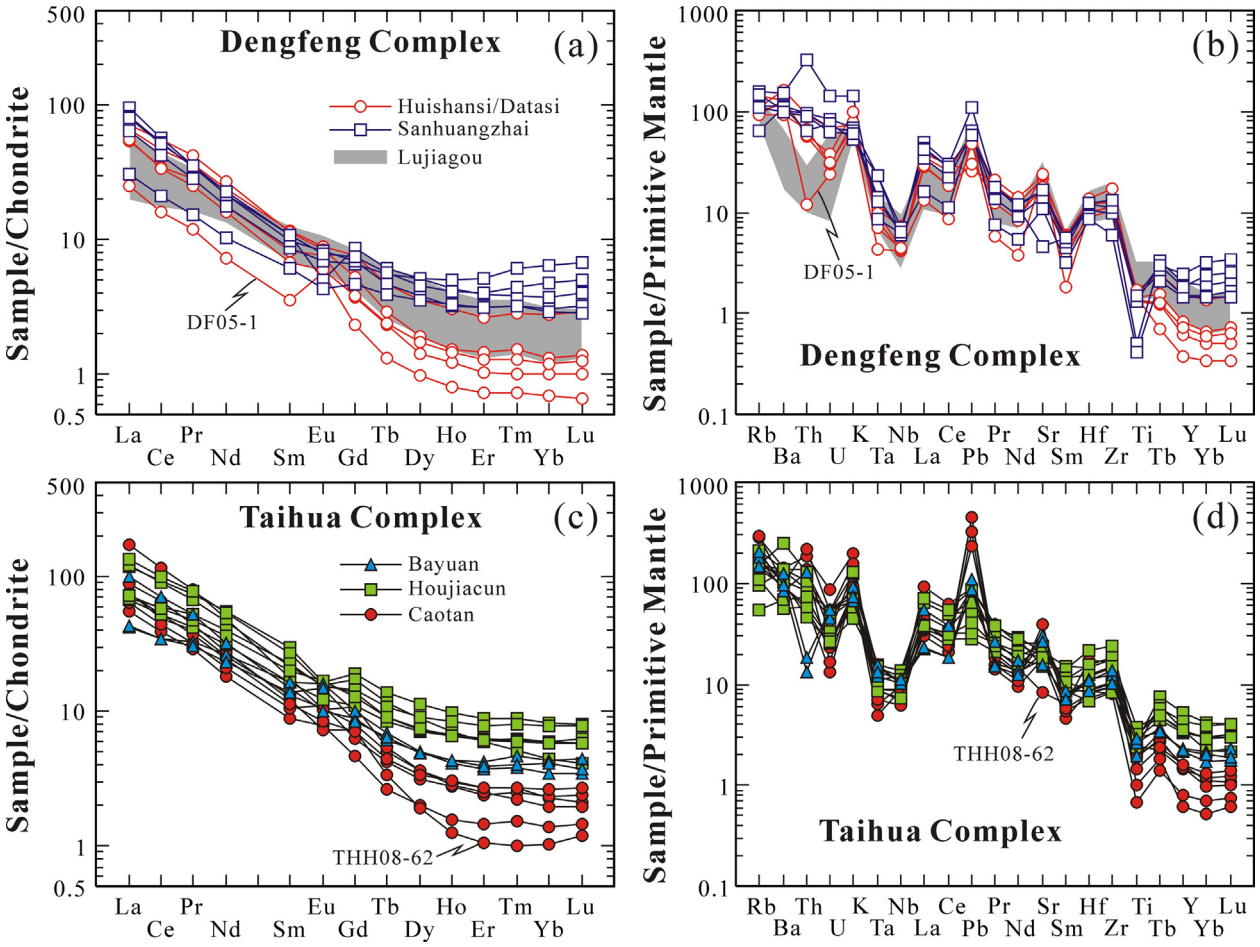

Fig. 7. Chondrite-normalized REE patterns and primitive mantle-normalized trace element spidergrams for TTG gneisses from (a and b) the Dengfeng Complex and (c and d) the Taihua Complex in the Xiaoqinling area. Chondrite and PM normalization factors are from Taylor and McLennan (1985) and Sun and McDonough (1989), respectively; the Lujiagou TTG gneisses are from Diwu et al. (2011).

The highly fractionated REE patterns and depletion in heavy REEs of the Dengfeng TTG (Fig. 7a) require generation of melts at depths where residual garnet and/or amphibole are stable (Fig. 10). Although many tectonic models have been proposed to satisfy this requirement, most early Archean and many late Archean TTG suites more likely represent partial melts of basaltic lower crust rather than subducted/subducting ocean crust (Smithies and Champion, 2000; Smithies, 2000; Condie, 2005). The Dengfeng TTG gneisses all have high SiO_2, low MgO ($Mg^{\#}$), Cr and Ni (Fig. 5), indicating that thickened lower crust might be a more suitable source than the subducting ocean crust or delaminated eclogite, because the latter would induce high MgO ($Mg^{\#}$), Cr and Ni in the melts (e.g., Rapp et al., 1999; Smithies, 2000; Martin et al., 2005; Wang et al., 2006). High Rb/Sr ratios (>0.1; Table 1) of the Dengfeng TTG gneisses are also compatible with melts derived from thickened mafic crust (Huang et al., 2009), in contrast to the generally low Rb/Sr ratios (<0.05) in adakites derived from slab melts (Huang et al., 2009). As deduced from the Nd and Hf isotopic systems, petrogenesis of the Dengfeng TTG gneisses requires the participation of both juvenile components and pre-existing crustal material. Thus the partial melting of thickened lower crust is the favored mechanism for generating the Dengfeng TTG.

6.1.2. Petrogenesis of the TTG gneisses of the Taihua Complex in the Xiaoqinling area

The Xiaoqinling TTG gneisses at Caotan, Houjiacun and Bayuan all show depletion in heavy REE and Y, with high Sr/Y and La/Yb ratios (Fig. 7; Table 1), indicating the partial melting process was at pressures high enough to stabilize garnet ± amphibole. Sr/Y and La/Yb in the melt could increase significantly as a result of fractionation of amphibole and/or garnet at such pressures (Macpherson et al., 2006), but this would also lead to positive correlation between the Sr/Y and La/Yb ratios (Huang et al., 2012). Given the lack of Sr/Y correlation with La/Yb for the Houjiacun and Bayuan TTG gneisses (Table 1), it suggests that the high Sr/Y and La/Yb in these rocks are not due to amphibole and/or garnet fractionation, but can be attributed to partial melting, leaving residual amphibole and/or garnet in the source (Fig. 10). The overall low Dy/Yb ratios (Dy/Yb < 2.5, except for a few granite gneiss samples from the Houjiacun and Bayuan TTG gneisses; Table 1), indicate that both amphibole and garnet were residual during partial melting (e.g., PM-2 in Fig. 10). The Caotan TTG gneisses have variable Sr/Y and La/Yb ratios, which is attributed not only to amphibole and/or garnet fractionation, but also to plagioclase accumulation or fractionation (Fig. 10).

The Caotan TTG gneisses have low $Mg^{\#}$ and Cr and Ni contents (Table 1), which is different from typical subducted oceanic crust-derived adakites or partial melts of delaminated lower crust, but similar to those derived from thickened lower crust (Fig. 5). Abundant inherited zircons in tonalite sample THH05-97 (Fig. 3c and d) also indicate that the Caotan TTGs result from partial melting of pre-existing crustal materials. Thus the partial melting of thickened lower crust is the favored mechanism for generating the Caotan TTG.

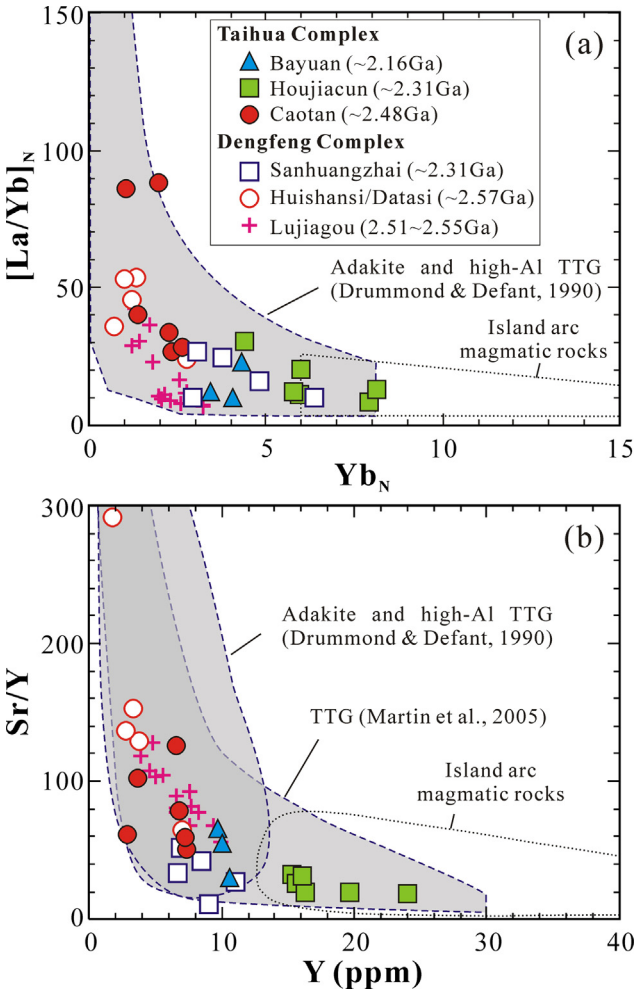

Fig. 8. Plots of (a) $(La/Yb)_N$ versus Yb_N and (b) Sr/Y versus Y for TTG gneisses from the Dengfeng and Taihua Complexes in the Xiaoqinling area. Fields of high-Al TTG, adakite and island arc magmatic rocks are from Defant and Drummond (1990) and Martin et al. (2005); the Lujiagou TTG gneisses are from Diwu et al. (2011).

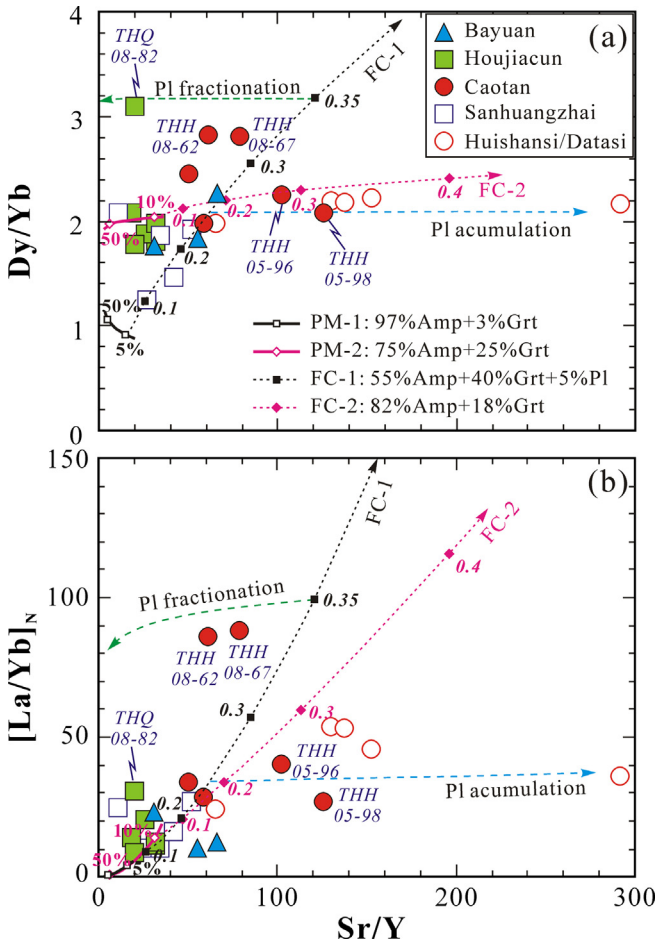

Fig. 10. Diagrams showing relationships of (a) Dy/Yb versus Sr/Y and (b) $[La/Yb]_N$ versus Sr/Y for the gneisses in the Dengfeng and Taihua Complexes. Partial melting curves of N-MORB (PM-1, PM-2) and Rayleigh fractional crystallization curve (FC-1: 5% melts on PM-1; FC-2: 10% melts on PM-2) were calculated by using partition coefficients in the system of andesitic to tonalitic melts: amphibole (Sisson, 1994), garnet (Barth et al., 2002), plagioclase (Drake and Weill, 1975). The N-MORB average is from Hofmann (1988).

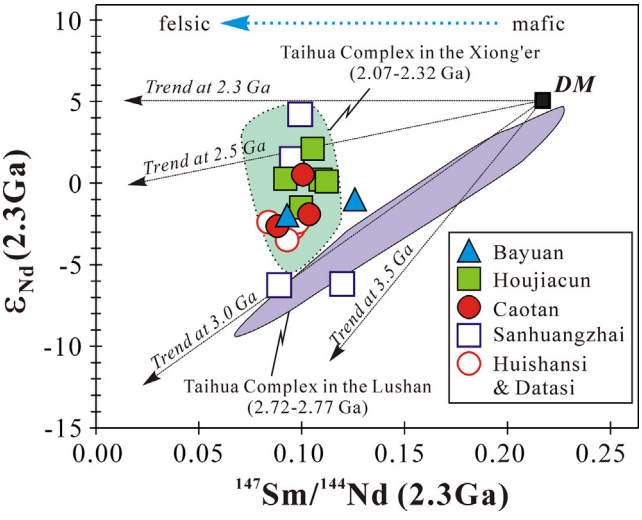

Fig. 9. Nd isotopic evolution diagram for the TTG gneisses in the Dengfeng Complex and Taihua Complex in the Xiaoqinling area. The field of gneisses in the Taihua Complex in the Lushan (Huang et al., 2010) and Xiong'er (Huang et al., 2012) areas are also shown for comparison.

MgO ($Mg^{\#}$), Ni and Cr of most Houjiacun samples are similar to the Caotan TTG samples and in the range of lower crust-derived adakitic rocks or experimental melts of natural hydrous basalts at 1–4 GPa (Fig. 5a, f and g), indicating that the Houjiacun samples would also be derived from partial melting of the thickened lower crust, which is compatible with the mostly negative zircon $\varepsilon_{Hf}(t_{7/6})$ values (Fig. 4b) and old $T_{DM\text{-}Hf}{}^{C}$ (2.75–3.19 Ga; Supplemental Table 3).

The Bayuan TTG gneisses have high MgO ($Mg^{\#}$), Ni and Cr (Fig. 5), which is consistent with partial melting of subducted oceanic crust or delaminated lower crust. Given that all samples show negative whole rock $\varepsilon_{Nd}(t)$ (−3.85 to −2.33) and zircon $\varepsilon_{Hf}(t_{7/6})$ values (−7.81 to −1.99), corresponding to much older whole rock Nd model ages (2.74–2.82 Ga) and zircon "crustal" model ages (2.86–3.22 Ga) than their crystallization age (2168 ± 13 Ma), the partial melting of delaminated lower crust is the preferred mechanism. Additionally, the high Rb/Sr ratios (0.17–0.35; Table 1) also suggest a large contribution of the lower crust in their generation (Huang et al., 2009). The lower crust might form at ~2.3 Ga according to the ages of inherited zircons (Fig. 3b).

6.2. Orogeny in the Late Neoarchean and Early Paleoproterozoic

There are widespread Late Neoarchean TTG gneisses in the Dengfeng Complex. Wan et al. (2009) obtained a weighted mean $^{207}Pb/^{206}Pb$ age of 2531 ± 9 Ma from the Datasi tonalite gneiss, which is slightly younger than the single-zircon evaporation $^{207}Pb/^{206}Pb$ age of 2557 ± 9 Ma obtained by Lao and Wang (1999). Thus the Datasi TTG rocks might have formed contemporaneous with, or shortly after, emplacement of the Huishansi TTG rocks (2568 ± 11 Ma; Fig. 2b). LA-ICPMS U–Pb dating of zircons from the Lujiagou TTG gneisses north of Junzhao (Fig. 1c) gave the crystallization ages of trondhjemite as 2510 ± 20 to 2521 ± 21 Ma and of the tonalite as 2544 ± 10 to 2587 ± 55 Ma (Diwu et al., 2011). The geochemical characteristics of the Lujiagou TTG gneisses are similar to those of the Huishansi and Datasi TTG gneisses (Figs. 5–8). Thus high SiO_2, low MgO ($Mg^{\#}$), Cr and Ni (Fig. 5) of the Late Neoarchean TTG gneisses in the Dengfeng Complex indicate the partial melting of thickened lower crust.

The Caotan TTG gneisses (2.48 Ga) of the Taihua Complex in the Xiaoqinling area are also characterized by low MgO ($Mg^{\#}$), Cr and Ni (Fig. 5), suggesting thickened crust in the area at the beginning of the Early Paleoproterozoic.

The Sanhuangzhai TTG (2306 ± 6 Ma; Fig. 2d) is the only identified Early Paleoproterozoic felsic intrusion in the Dengfeng Complex, similar to the Houjiacun TTG (2.31 Ga; Fig. 3h and j) in the Xiaoqinling area and the Tieluping/Muce TTGs in the Xiong'er area (2.30–2.32 Ga; Huang et al., 2012) of the Taihua Complex. To explain the low MgO, Cr and Ni of these rocks (Fig. 5), thickened lower crust is also proposed as the source.

Therefore, the Dengfeng and Taihua TTGs at 2.30–2.57 Ga are all partial melts of thickened lower crust, which might have formed through orogeny (e.g., Burg and Ford, 1997), repeated underplating (e.g., Furlong and Fountain, 1986; Haschke et al., 2002), intra-oceanic plate stacking (De Wit, 1998), and/or oceanic plateau accretion (e.g., De Wit et al., 1992; Desrochers et al., 1993; Condie, 1997). The last two processes would produce dominantly juvenile crust, which contradicts the abundant inherited zircons and negative whole rock $\varepsilon_{Nd}(t)$ and zircon $\varepsilon_{Hf}(t)$ values recorded by the Dengfeng and Xiaoqinling TTGs. The thickening of crust by repeated underplating would be a long-term process and result in evolutionary changes in geochemical and isotopic characteristics (Haschke et al., 2002), which is different from the uniform age of inherited zircons in the Xiaoqinling TTGs (Fig. 3). The most effective thickening process would be tectonic shortening due to convergence between two plates (Giese et al., 1999). In the southern NCC, the Late Neoarchean and Early Paleoproterozoic accretionary orogeny probably occurred through slab-subduction. Therefore, the Dengfeng and Taihua TTGs at 2.30–2.57 Ga indicate that at least two episodic orogeny processes (2.48–2.57 and 2.31 Ga) were operative in the southern segment of the TNCO during the Late Neoarchean and Early Paleoproterozoic.

6.3. Orogenic collapse at the end of the Early Paleoproterozoic

The Bayuan TTGs have high MgO ($Mg^{\#}$), Ni and Cr, and would be derived from partial melting of delaminated lower crust. Delamination is a process where by a dense segment of the lower crust and lithospheric mantle sink into the convecting asthenosphere as a result of their negative buoyancy (Rudnick and Fountain, 1995). For delamination to occur, the lower crust must undergo large density increases, which is always due to "eclogitic" phase transitions (Kay and Kay, 1993; Lustrino, 2005). The lower crust might have been thickened enough for partial melting to occur, with a restite of eclogite or garnet-clinopyroxenite (Kay and Kay, 1993), and partial melts of TTG and adakitic affinity (Lustrino, 2005). Extensive TTGs generated at ~2.48 Ga (Caotan area) or at ~2.31 Ga (Houjiacun area) suggest that the lower crust beneath the orogenic belt in the Xiaoqinling area had been overall "eclogitic" character in the Early Paleoproterozoic, which would be responsible for delamination or detachment of the lower crust at the end of the Early Paleoproterozoic (such as the Bayuan TTG at ~2.16 Ga). During sinking, the lower crust is likely to undergo partial melting, producing liquids of TTG or adakitic affinity (e.g., Zegers and van Keken, 2001; Xu et al., 2002; Lustrino, 2005).

The highly dense eclogites inducing lithospheric delamination are always formed in orogenic settings (e.g., Lustrino, 2005). Thus the Bayuan TTG formed by partial melting of delaminated lower crust might record orogenic collapse in the Xiaoqinling area. Orogenic collapse at the end of the Early Paleoproterozoic is likely to be an important stage in the continental evolution of the southern segment of the TNCO. For example, the later episode of magmatism (2.19–2.07 Ga) in the Xiong'er area of the Taihua Complex is potassium-rich, suggesting an extensional regime as a consequence of post-collisional uplift at the end of the Early Paleoproterozoic (Huang et al., 2012).

6.4. Episodic crustal accretion in the southern NCC

It has been suggested that the Taihua Complex in the Xiaoqinling area is comparable with the Taihua Complex in other areas, based on Sm–Nd data and depleted mantle Nd model ages, Ar–Ar dating and single-grain zircon evaporation Pb–Pb ages (BGMR, 1982; Qi, 1992; Zhou et al., 1998). The zircon U–Pb data acquired here for the TTG gneisses of the Taihua Complex in the Xiaoqinling area reveal three episodes of crystallization (~2.48 Ga, ~2.31 Ga and ~2.16 Ga), distinctly different from the Taihua Complex in the Lushan area that mostly formed in the Late Mesoarchean and Early Neoarchean (Liu et al., 2009; Huang et al., 2010). The Early Paleoproterozoic TTGs from Houjiacun (2.31 Ga) and Bayuan (2.16 Ga) might be comparable with events in the Xiong'er area of the Taihua Complex that consists of potassium-rich igneous rock at 2.07–2.19 Ga and TTGs at 2.30–2.32 Ga (Huang et al., 2012), but the Taihua Complex in the Xiaoqinling area is characterized by magmatism at the end of the Late Neoarchean and the beginning of the Early Paleoproterozoic, with a crystallization age of 2477 ± 8 Ma and an inherited zircon age of 2552 ± 4 Ma for the tonalite sample from Caotan. Therefore, the Taihua Complex in different areas likely records distinct magmatic activities.

The Dengfeng Complex also records magmatic activity of the Late Neoarchean (2.57–2.49 Ga; Wan et al., 2009; Diwu et al., 2011; Zhang et al., 2013; this study) and in the Early Paleoproterozoic (~2.31 Ga; Fig. 2d), with TTGs of the Dengfeng Complex generated through partial melting of thickened lower crust. The TTGs in the Xiaoqinling area formed at ~2.55 to 2.48 Ga at Caotan and ~2.31 Ga at Houjiacun by a similar formation mechanism. So there are some comparable features between the Dengfeng Complex and the Taihua Complex in the Xiaoqinling area.

Episodic magmatic activity (2.85–2.72 Ga, 2.57–2.48 Ga, 2.32–2.30 Ga and 2.20–2.07 Ga; Fig. 11a and Table 3) is recorded from the southern segment of the TNCO and extends from the Late Archean to Early Paleoproterozoic, based on combined geochronological evidence from the Dengfeng Complex (the Dengfeng area) and the Taihua Complex (including the Lushan, Xiong'er and Xiaoqinling areas). The Taihua Complex in the Lushan area formed in the Late Mesoarchean and Early Neoarchean (Liu et al., 2009; Huang et al., 2010) and probably records the earliest episode of magmatism in the southern segment of the TNCO. The second episode is recorded mainly in the Dengfeng and Xiaoqinling areas and is Late Neoarchean in age. It continued in the Xiaoqinling area to the beginning of the Early Paleoproterozoic. Magmatism of the third episode occurred in the Dengfeng, Xiong'er and Xiaoqinling areas with a peak at 2310 Ma (Fig. 11a). Magmatism of the last

Table 3
Zircon U–Pb dating results of the Taihua and Dengfeng Complexes.

Sample	Rocks	Age (Ma)	Methods	References
The Taihua Complex in the Xiaoqinling area				
THB05-103	Tonalite gneiss	2164 ± 16	SHRIMP, mean $^{207}Pb/^{206}Pb$ age	This study
THH05-97	Tonalite gneiss	2477 ± 8	SHRIMP, mean $^{207}Pb/^{206}Pb$ age	This study
		2552 ± 4	SHRIMP, mean $^{207}Pb/^{206}Pb$ age (inherited zircons)	This study
		1912 ± 12	SHRIMP, apparent $^{207}Pb/^{206}Pb$ age (metamorphic zircon)	This study
THH08-62	Granitic gneiss	2477 ± 28	CAMECA, mean $^{207}Pb/^{206}Pb$ age	This study
		1918 ± 17	CAMECA, upper intercept age (metamorphic zircon)	This study
THQ08-76	Tonalite gneiss	2311 ± 3	CAMECA, mean $^{207}Pb/^{206}Pb$ age	This study
THQ08-82	Granitic gneiss	2307 ± 5	CAMECA, mean $^{207}Pb/^{206}Pb$ age	This study
The Taihua Complex in the Xiong'er area				
THX05-41	Tonalite gneiss	2065 ± 23	SHRIMP, mean $^{207}Pb/^{206}Pb$ age	Huang et al. (2012)
THX05-45	Kfs granitic gneiss	2188 ± 26	SHRIMP, mean $^{207}Pb/^{206}Pb$ age	Huang et al. (2012)
THX08-57	Granodioritic gneiss	2318 ± 8	CAMECA, mean $^{207}Pb/^{206}Pb$ age	Huang et al. (2012)
THX08-54	Dioritic gneiss	2305 ± 23	CAMECA, mean $^{207}Pb/^{206}Pb$ age	Huang et al. (2012)
MC-12	Gneiss	2336 ± 13	LA-ICPMS, upper intercept age	Diwu et al. (2007)
MC-19	Gneiss	2316 ± 16	LA-ICPMS, upper intercept age	Diwu et al. (2007)
The Taihua Complex in the Lushan area				
LS0417-1	Banded amphibolite	2838 ± 35	SHRIMP, mean $^{207}Pb/^{206}Pb$ age	Liu et al. (2009)
		2792 ± 11	SHRIMP, mean $^{207}Pb/^{206}Pb$ age (metamorphic zircons)	Liu et al. (2009)
LS0417-3	Gneissic amphibolite	2845 ± 23	SHRIMP, mean $^{207}Pb/^{206}Pb$ age	Liu et al. (2009)
		2776 ± 20	SHRIMP, mean $^{207}Pb/^{206}Pb$ age (metamorphic zircons)	Liu et al. (2009)
LS0417-2	Gneissic tonalite	2829 ± 18	SHRIMP, mean $^{207}Pb/^{206}Pb$ age	Liu et al. (2009)
		2772 ± 22	SHRIMP, mean $^{207}Pb/^{206}Pb$ age (metamorphic zircons)	Liu et al. (2009)
LS0417-4	Gneissic tonalite	2832 ± 11	SHRIMP, mean $^{207}Pb/^{206}Pb$ age	Liu et al. (2009)
		2772 ± 17	SHRIMP, mean $^{207}Pb/^{206}Pb$ age (metamorphic zircons)	Liu et al. (2009)
THL05-2	Tonalite gneiss	2765 ± 13	SHRIMP, upper intercept age	Huang et al. (2010)
THL05-21	Tonalite gneiss	2723 ± 9	SHRIMP, upper intercept age	Huang et al. (2010)
		1917 ± 37	SHRIMP, apparent $^{207}Pb/^{206}Pb$ age (metamorphic zircon)	Huang et al. (2010)
TWJ358/1	Gneissic granite	2139 ± 16	SHRIMP, concordian age	Wan et al. (2006)
The Dengfeng Complex				
DF08-7	Tonalite gneiss	2306 ± 6	CAMECA, mean $^{207}Pb/^{206}Pb$ age	This study
DF05-9	Granodiorite gneiss	2568 ± 11	SHRIMP, upper intercept age	This study
DF07-08	Trondhjemite gneiss	2521 ± 21	LA-ICPMS, upper intercept age	Diwu et al. (2011)
DF07-10	Trondhjemite gneiss	2510 ± 20	LA-ICPMS, upper intercept age	Diwu et al. (2011)
DF07-15	Tonalite gneiss	2547 ± 17	LA-ICPMS, mean $^{207}Pb/^{206}Pb$ age	Diwu et al. (2011)
DF07-24	Tonalite gneiss	2544 ± 10	LA-ICPMS, upper intercept age	Diwu et al. (2011)
09DF-18	Amphibolite	2547 ± 14	LA-ICPMS, upper intercept age	Diwu et al. (2011)
09DF-19	Metadiorite	2529 ± 14	LA-ICPMS, upper intercept age	Diwu et al. (2011)
XS0416-12	Trondhjemite gneiss	2553 ± 8	SHRIMP, mean $^{207}Pb/^{206}Pb$ age	Wan et al., 2009
XS0416-11	Potassium granite	2513 ± 33	SHRIMP, upper intercept age	Wan et al. (2009)
XS0416-10	Tonalite gneiss	2531 ± 9	SHRIMP, mean $^{207}Pb/^{206}Pb$ age	Wan et al. (2009)
XS0416-6	Quartz schist	2508 ± 16	SHRIMP, mean $^{207}Pb/^{206}Pb$ age	Wan et al. (2009)
XS0416-7	Quartz schist	2531 ± 15	SHRIMP, mean $^{207}Pb/^{206}Pb$ age	Wan et al. (2009)
XS0416-8	Meta-quartz keratophyre	2522 ± 12	SHRIMP, mean $^{207}Pb/^{206}Pb$ age	Wan et al. (2009)
WZJ84015	Metadiorite	2493 ± 7	SHRIMP, mean $^{207}Pb/^{206}Pb$ age	Wang et al. (2004)
SPH1101	Diorite gneiss	2506 ± 5	LA-ICPMS, mean $^{207}Pb/^{206}Pb$ age	Zhang et al. (2013)
SPH1102	Diorite gneiss	2516 ± 18	LA-ICPMS, mean $^{207}Pb/^{206}Pb$ age	Zhang et al. (2013)
SPH1103	Diorite gneiss	2504 ± 4	LA-ICPMS, mean $^{207}Pb/^{206}Pb$ age	Zhang et al. (2013)
SPH1104	Plagioclase amphibolite	2502 ± 4	LA-ICPMS, mean $^{207}Pb/^{206}Pb$ age	Zhang et al. (2013)
SPH1105	Plagioclase amphibolite	2504 ± 5	LA-ICPMS, mean $^{207}Pb/^{206}Pb$ age	Zhang et al. (2013)
SC1103	Plagioclase amphibolite	2506 ± 21	LA-ICPMS, mean $^{207}Pb/^{206}Pb$ age	Zhang et al. (2013)

episode at 2.19–2.07 Ga is rare and sporadic in the Lushan, Xiong'er and Xiaoqinling areas. No magmatism has been observed so far in the southern segment of the TNCO during the time-intervals of 2.72–2.57 Ga, 2.48–2.32 Ga and 2.30–2.20 Ga (Fig. 11a), indicating periods of quiescence.

The magmatic rocks of the first two episodes consist dominantly of juvenile compositions as shown by dominantly positive whole rock $\varepsilon_{Nd}(t)$ and zircon $\varepsilon_{Hf}(t)$ values (Figs. 11b and c), suggesting two episodes of crustal growth from the Late Mesoarchean to the beginning of the Early Paleoproterozoic in the southern segment of the TNCO, which are contemporaneous with the two main crustal growth episodes recognized in the NCC (2.9–2.7 Ga and 2.55–2.50 Ga; Zhai et al., 2010). Juvenile continental crust is produced at subduction zones or by mantle plumes (Condie, 1998). Late Mesoarchean to Early Neoarchean crustal growth in the southern segment of the TNCO was mostly achieved through the partial melting of subducted ocean crust (Huang et al., 2010), suggesting early plate subduction in the southern segment of the TNCO. The Late Neoarchean Dengfeng TTGs formed through subduction processes, and the Shipaihe metadiorites at 2.49 are typical high-K intermediate rocks and indicate subduction extending from the end of the Neoarchean into the Paleoproterozoic (Diwu et al., 2011). The Caotan TTGs in the Xiaoqinling area of the Taihua Complex formed by the partial melting of thickened lower crust, probably also indicating subduction processes. Therefore, crustal growth from the Late Neoarchean to the beginning of the Early Paleoproterozoic was related to subduction.

The third episode of magmatism at ~2.31 Ga consists of both juvenile and pre-existing crustal materials, as shown by its large variable whole rock $\varepsilon_{Nd}(t)$ and zircon $\varepsilon_{Hf}(t)$ values (Figs. 11b and c). A large proportion of pre-existing crustal materials with negative whole rock $\varepsilon_{Nd}(t)$ and zircon $\varepsilon_{Hf}(t)$ values were derived from the continental crust formed during the first episode of magmatism (Fig. 11b and c). Subduction might have restarted along the southern margin of the North China Craton after a period of quiescence. This later event would not only add juvenile components, but also trigger the partial melting of pre-existing lower crustal materials. It is commonly accepted that the assembly of the Columbia

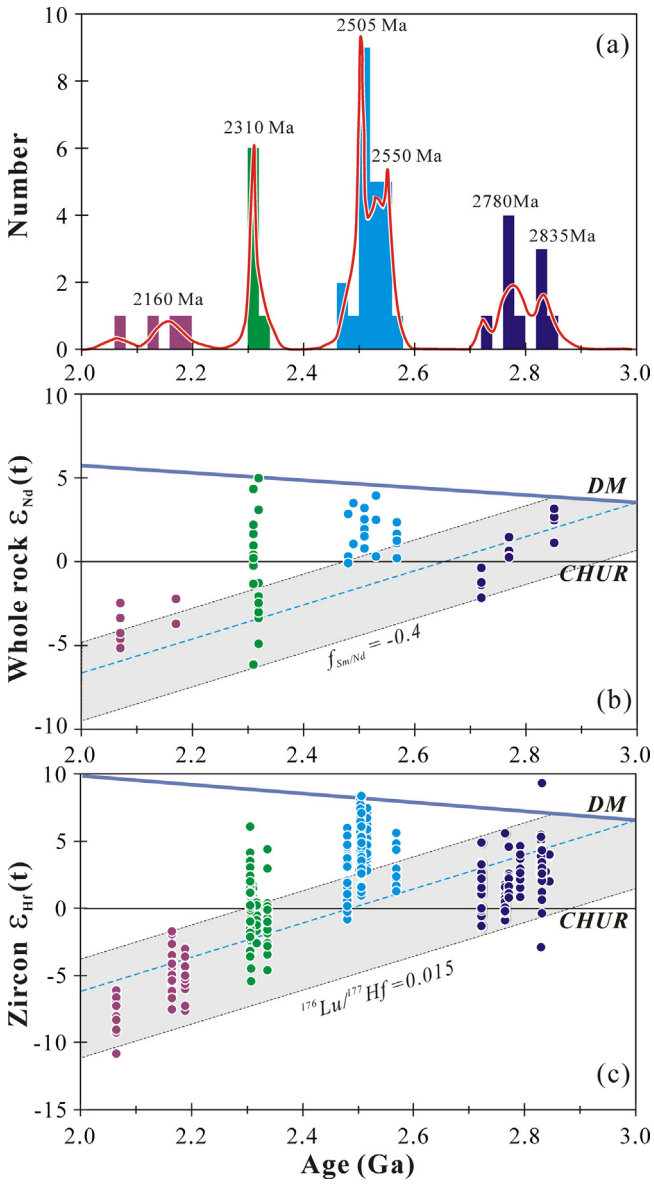

Fig. 11. Distribution of (a) zircon U–Pb ages, (b) whole rock $\varepsilon_{Nd}(t)$ values and (c) zircon $\varepsilon_{Hf}(t)$ values for the Dengfeng and Taihua Complexes in the southern segment of the TNCO. Zircon U–Pb ages are listed in Table 3. Whole rock Nd isotopes are from Zhang and Li (1988), Wan et al. (2009), Huang et al. (2010, 2012), Zhou et al. (2009, 2011) and this paper. Zircon Hf isotopes are from Liu et al. (2009), Huang et al. (2010, 2012), Zhang et al. (2013) and this paper.

supercontinent was completed by global-scale collisional events in the period 2.0–1.8 Ga (e.g., Zhao et al., 2002b, 2004, 2011). The North China Craton, as a likely component of the Columbia supercontinent, was also probably involved in this event (Zhao et al., 2003b, 2011). If our interpretation about subduction at ~2.31 Ga is correct, it would record the initial subduction in the southern North China Craton related to the assembly of the Columbia supercontinent.

The final episode of magmatism (2.2–2.0 Ga) was contemporary with the breakup of the first proposed supercontinent that aggregated in the Late Archean (Condie, 1998) or the assembly of the Early Proterozoic supercontinent (i.e. Columbia/Nuna) (Condie, 1998). Magmatism reveals an absence of juvenile materials and is characterized by negative whole rock $\varepsilon_{Nd}(t)$ and zircon $\varepsilon_{Hf}(t)$ values (Fig. 11b and c). It was thus a period of crustal reworking, rather than one of crustal addition.

In brief, there are three episodes of continental growth in the southern segment of the TNCO at 2.85–2.72 Ga, 2.57–2.48 Ga and 2.34–2.30 Ga caused by crustal thickening through slab subduction and accretionary orogeny, and one episode of crustal reworking (2.2–2.0 Ga) due to orogenic collapse. This is consistent with a globally significant period of plate tectonics. Additionally, the Taihua Complex in the Lushan and Xiaoqinling areas have metamorphic ages of ~1.91 Ga (Table 3), similar to the metamorphic recrystallization age of the lower crust (1915 ± 27 Ma) defined by the Nushan granulite xenoliths in the southern NCC (Huang et al., 2004). This metamorphic age is earlier than that of the central and northern segments of the TNCO recorded by the Lüliang, Fuping, Wutai, Hengshan, Zanhuang, Xuanhua and Huai'an complexes (mostly 1.88–1.80 Ga; Zhao and Zhai, 2013), which might suggest an asynchronous amalgamation of the NCC along the TNCO in the Paleoproterozoic.

7. Conclusions

The Taihua Complex in the Xiaoqinling area formed mainly in the Early Paleoproterozoic, including three episodes of TTG magmatism (~2.48 Ga, ~2.31 Ga and ~2.16 Ga). Both the Caotan TTGs at ~2.48 Ga and the Houjiacun TTGs at ~2.31 Ga were derived from the partial melting of thickened lower crust with residual garnet and amphibole. The Bayuan TTGs at ~2.16 Ga were the result of partial melting of delaminated lower crust that underwent interaction with peridotite mantle.

The Dengfeng Complex contains dominantly Late Neoarchean TTG gneisses (2.53–2.57 Ga) and lesser amounts of Early Paleoproterozoic TTG gneisses (2.31 Ga). Both the Late Neoarchean and Early Paleoproterozoic TTG gneisses resulted from the partial melting of thickened lower crust with residual garnet and amphibole.

There were at least four episodes of magmatic activity in the southern segment of the TNCO extending from the Late Mesoarchean to Early Paleoproterozoic (2.85–2.72 Ga, 2.57–2.48 Ga, 2.34–2.30 Ga and 2.20–2.07 Ga). The three earlier episodes of magmatism recorded episodic continental growth through plate subduction and consequent orogeny in the southern segment of the TNCO, consistent with globally recognized periods of plate accretion. The last episode of magmatism was attributed to crustal reworking during orogenic collapse.

Acknowledgements

We thank Q.L. Li for assistance with zircon CAMECA U–Pb dating, B. Song for SHRIMP zircon U–Pb dating, Y.H. Yang for zircon Lu–Hf isotope analyses, Y. Liu for major element analyses, X.L. Tu for trace element analyses and X.R. Liang for Nd isotope analyses. We acknowledged G.C. Zhao for critical comments significantly improving this contribution. This research was supported by the National Basic Research Program of China, (973 Program: 2012CB416703), National Natural Science Foundation of China (NSFC Projects 41130314, 91214202, 41121002). This is contribution No. IS-1685 to GIGCAS and contribution No. 467 to TIGeR (The Institute for Geoscience Research).

Appendix A. Supplementary data

Supplementary data associated with this article can be found, in the online version, at http://dx.doi.org/10.1016/j.precamres.2013.05.016.

References

Barker, F., Arth, J.G., 1976. Generation of trondhjemitic–tonalitic liquids and Archaean bimodal trondhjemite–basalt suites. Geology 4, 596–600.

Barth, M.G., Foley, S.F., Horn, I., 2002. Partial melting in Archean subduction zones: constraints from experimentally determined trace element partition coefficients between eclogitic minerals and tonalitic melts under upper mantle conditions. Precambrian Research 113, 323–340.
Bédard, J.H., 2006. A catalytic delamination-driven model for coupled genesis of Archaean crust and sub-continental lithospheric mantle. Geochimica et Cosmochimica Acta 70, 1188–1214.
BGMR (Bureau of Geology and Mineral Resources), 1965. Geological Map of Henan Province. Sheet I-49-XVII (Linru) and I-49-XVIII (Xuchang) Scale 1:200,000. Bureau of Geology and Mineral Resources of Henan Province, Zhengzhou.
BGMR (Bureau of Geology and Mineral Resources), 1968. Geological Map of Shanxi Province. Sheet I-49-14 (Weinan) and I-49-15 (Luonan) Scale 1:200,000. Bureau of Geology and Mineral Resources of Shanxi Province, Xian.
BGMR (Bureau of Geology and Mineral Resources), 1982. Regional Geology of Shaanxi Province, People's Republic of China. Geological Publishing House, Beijing.
Burg, J.-P., Ford, M., 1997. Orogeny Through Time: An Overview, Special Publications 121. Geological Society, London, pp. 1–17.
Chu, N.C., Taylor, R.N., Chavagnac, V., Nesbitt, R.W., Boella, R.M., Milton, J.A., German, C.R., Bayon, G., Burton, K., 2002. Hf isotope ratio analysis using multi-collector inductively coupled plasma mass spectrometry: an evaluation of isobaric interference corrections. Journal of Analytical Atomic Spectrometry 17, 1567–1574.
Condie, K.C., 1997. Contrasting sources for upper and lower continental crust: the greenstone connection. The Journal of Geology 105, 729–736.
Condie, K.C., 1998. Episodic continental growth and supercontinents: a mantle avalanche connection? Earth and Planetary Science Letters 163, 97–108.
Condie, K.C., 2005. TTGs and adakites: are they both slab melts? Lithos 80, 33–44.
De Wit, M.J., 1998. On Archean granites, greenstones, cratons and tectonics: does the evidence demand a verdict? Precambrian Research 91, 181–226.
De Wit, M.J., Roering, C., Hart, R.J., Armstrong, R.A., de Ronde, C.E.J., Green, R.W.E., Tredoux, M., Peberdy, E., Hart, R.A., 1992. Formation of an Archaean continent. Nature 357, 553–562.
Defant, M.J., Drummond, M.S., 1990. Derivation of some modern arc magmas by melting of young subducted lithosphere. Nature 347, 662–665.
DePaolo, D.J., 1981. A neodymium and strontium isotopic study of the Mesozoic calc-alkaline granitic batholiths of the Sierra Nevada and Peninsular Ranges, California. Journal of Geophysical Research 86, 10470–10488.
Desrochers, J.P., Hubert, C., Ludden, J., Pilote, P., 1993. Accretion of Archean oceanic plateau fragments in the Abitibi greenstone belt, Canada. Geology 21, 451–454.
Ding, L.F., 1996. New recognition to Group Taihua in the Mountain Small Qinling in the west of province Henan. Journal of Xi'an College of Geology 18, 1–8 (in Chinese with English abstract).
Diwu, C.R., Sun, Y., Guo, A.L., Wang, H.L., Liu, X.M., 2011. Crustal growth in the North China Craton at ~2.5 Ga: evidence from in situ zircon U–Pb ages, Hf isotopes and whole-rock geochemistry of the Dengfeng Complex. Gondwana Research 20, 149–170.
Diwu, C.R., Sun, Y., Lin, C.L., Liu, X.M., Wang, H.L., 2007. Zircon U–Pb ages and Hf isotopes and their geological significance of Yiyang TTG gneisses from Henan province, China. Acta Petrologica Sinica 23, 253–262 (in Chinese with English abstract).
Drake, M.J., Weill, D.F., 1975. Partition of Sr, Ba, Ca, Y, Eu2+, Eu3+ and other REE between plagioclase feldspar and magmatic liquid: an experimental study. Geochimica et Cosmochimica Acta 39, 689–712.
Drummond, M.S., Defant, M.J., 1990. A model for trondhjemite–tonalite–dacite genesis and crustal growth via slab melting: Archean to modern comparisons. Journal of Geophysical Research 95, 21503–21521.
Furlong, K.P., Fountain, D.M., 1986. Continental crustal underplating: thermal considerations and seismic-petrologic consequences. Journal of Geophysical Research 91, 8285–8294.
Giese, P., Scheuber, E., Schilling, F., Schmitz, M., Wigger, P., 1999. Crustal thickening processes in the Central Andes and the different natures of the Moho-discontinuity. Journal of South American Earth Sciences 12, 201–220.
Griffin, W.L., Belousova, E.A., Shee, S.R., Pearson, N.J., O'Reilly, S.Y., 2004. Archean crustal evolution in the northern Yilgarn Craton: U–Pb and Hf-isotope evidence from detrital zircons. Precambrian Research 131, 231–282.
Griffin, W.L., Pearson, N.J., Belousova, E., Jackson, S.E., O'Reilly, S.Y., van Achterberg, E., Shee, S.R., 2000. The Hf isotope composition of cratonic mantle: LAM-MC-ICPMS analysis of zircon megacrysts in kimberlites. Geochimica et Cosmochimica Acta 64, 133–147.
Griffin, W.L., Pearson, N.J., Belousova, E.A., Saeed, A., 2006. Comment: Hf-siotope heterogeneity in zircon 91500. Chemical Geology 233, 358–363.
Guan, B.D. (Ed.), 1996. The Precambrian-Lower Cambrian Geology and Metallogensis in the South Border of the North China Platform in Henan Province. Press of China University of Geosciences, Wuhan, pp. 1–328 (in Chinese with English abstract).
Guo, A.L., 1988. Relationships between the TTG gneisses and the greenstone belt in the Archean Defngfeng granite-greenstone terrane, central Henan and their implications for crustal evolution. Geological Review 34, 123–131 (in Chinese with English abstract).
Haschke, M., Siebel, W., Günther, A., Scheuber, E., 2002. Repeated crustal thickening and recycling during the Andean Orogeny in north Chile (21°–26°S). Journal of Geophysical Research 107, 2019, http://dx.doi.org/10.1029/2001JB000328.
Hofmann, A.W., 1988. Chemical differentiation of the earth: the relationship between mantle, continental crust, and oceanic crust. Earth and Planetary Science Letters 90, 297–314.
Huang, X.L., Niu, Y.L., Xu, Y.G., Yang, Q.J., Zhong, J.W., 2010. Geochemistry of TTG and TTG-like gneisses from Lushan-Taihua Complex in the southern North China Craton: implications for late Archean crustal accretion. Precambrian Research 182, 43–56.
Huang, X.L., Wilde, S.A., Yang, Q.J., Zhong, J.W., 2012. Geochronology and Petrogenesis of grey gneisses from the Taihua Complex at Xiong'er in the southern segment of the Trans-North China Orogen: implications for tectonic transformation in the Early Paleoproterozoic. Lithos 134, 236–252.
Huang, X.L., Xu, Y.G., Lan, J.B., Yang, Q.J., Luo, Z.Y., 2009. Neoproterozoic adakitic rocks from Mopanshan in the western Yangtze Craton: Partial melts of a thickened lower crust. Lithos 112, 367–381.
Huang, X.L., Xu, Y.G., Liu, D.Y., 2004. Geochronology, petrology and geochemistry of the granulite xenoliths from Nushan, east China: implication for a heterogeneous lower crust beneath the Sino-Korean craton. Geochimica et Cosmochimica Acta 68, 127–149.
Iizuka, T., Hirata, T., 2005. Improvements of precision and accuracy in in-situ Hf isotope microanalysis of zircon using the laser ablation-MC-ICPMS technique. Chemical Geology 220, 121–137.
Kay, R.W., Kay, S.M., 1993. Delamination and delamination magmatism. Tectonophysics 219, 177–189.
Kay, S.M., Ramos, V.A., Marquez, M., 1993. Evidence in Cerro Pampa volcanic rocks for slab-melting prior to ridge-trench collision in southern South America. The Journal of Geology 101, 703–714.
Keto, L.S., Jacobsen, S.B., 1987. Nd and Sr isotopic variations of Early Paleozoic oceans. Earth and Planetary Science Letters 84, 27–41.
Kröner, A., Compston, W., Zhang, G.W., Guo, A.L., Todt, W., 1988. Age and tectonic setting of late Archean greenstone-gneiss terrain in Henan Province, China, as revealed by single-grain zircon dating. Geology 16, 211–215.
Kusky, T.M., 2011. Geophysical and geological tests of tectonic models of the North China Craton. Gondwana Research 20, 26–35.
Kusky, T.M., Li, J.H., 2003. Paleoproterozoic tectonic evolution of the North China Craton. Journal of Asian Earth Sciences 22, 23–40.
Lao, Z.Q., Wang, S.Y., 1999. New advances in the study of the Dengfeng Complex in the Songshan region, Henan Province. Regional Geology of China 18, 9–16 (in Chinese with English abstract).
Li, S.G., Hart, S.R., Guo, A.L., Zhang, G.W., 1987. A whole-rock Sm–Nd age for the Dengfeng group in central Henan province and its tectonic implication. Chinese Science Bulletin 32, 1728–1731 (in Chinese).
Li, S.Z., Zhao, G.C., 2007. SHRIMP U-Pb zircon geochronology of the Liaoji granitoids: constraints on the evolution of the Paleoproterozoic Jiao-Liao-Ji belt in the Eastern Block of the North China Craton. Precambrian Research 158, 1–16.
Li, S.Z., Zhao, G.C., Sun, M., Wu, F.Y., Liu, J.Z., Hao, D.F., Han, Z.Z., Luo, Y., 2004. Mesozoic, not Paleoproterozoic SHRIMP U–Pb zircon ages of two Liaoji granites, Eastern Block, North China Craton. International Geology Review 46, 162–176.
Li, S.Z., Zhao, G.C., Sun, M., Han, Z.Z., Zhao, G.T., Hao, D.F., 2006a. Are the South and North Liaohe Groups of the North China Craton different exotic terranes? Nd isotope constraints. Gondwana Research 9, 198–208.
Li, X.H., Li, Z.X., Wingate, M.T.D., Chung, S.L., Liu, Y., Lin, G.C., Li, W.X., 2006b. Geochemistry of the 755 Ma Mundine Well dyke swarm, northwestern Australia: part of a Neoproterozoic mantle superplume beneath Rodinia? Precambrian Research 146, 1–15.
Li, X.H., Liu, Y., Li, Q.L., Guo, C.H., Chamberlain, K.R., 2009. Precise determination of Phanerozoic zircon Pb/Pb age by multicollector SIMS without external standardization. Geochemistry Geophysics Geosystems 10, Q04010, http://dx.doi.org/10.1029/2009GC002400.
Li, X.P., Yang, Z.Y., Zhao, G.C., Grapes, R., Guo, J.H., 2011. Geochronology of khondalite-series rocks of the Jining Complex: confirmation of depositional age and tectonometamorphic evolution of the North China Craton. International Geology Review 53, 1194–1211.
Liu, C.H., Zhao, G.C., Sun, M., Zhang, J., Yin, C.Q., 2012a. U–Pb geochronology and Hf isotope geochemistry of detrital zircons from the Zhongtiao Complex: constraints on the tectonic evolution of the Trans-North China Orogen. Precambrian Research 222/223, 159–172.
Liu, C.H., Zhao, G.C., Sun, M., Zhang, J., Yin, C.Q., He, Y.H., 2012b. Detrital zircons U–Pb dating, Hf isotope and whole-rock geochemistry from the Songshan Group in the Dengfeng Complex: constraints on the tectonic evolution of the Trans-North China Orogen. Precambrian Research 192, 1–15.
Liu, D.Y., Nutman, A.P., Compston, W., Wu, J.S., Shen, Q.H., 1992. Remnants of 3800 Ma crust in the Chinese Part of the Sino-Korean craton. Geology 20, 339–342.
Liu, D.Y., Wilde, S.A., Wan, Y.S., Wang, S.Y., Valley, J.W., Kita, N., Dong, C.Y., Xie, H.Q., Yang, C.X., Zhang, Y.X., Gao, L.Z., 2009. Combined U–Pb, hafnium and oxygen isotope analysis of zircons from meta-igneous rocks in the southern North China Craton reveal multiple events in the Late-Mesoarchean-Early Neoarchean. Chemical Geology 261, 140–154.
Ludwig, K.R., 2001. SQUID 1.02: A User's Manual. Berkeley Geochronology Center. Special Publication No. 2.
Ludwig, K.R., 2003. Isoplot: A Geochronological Toolkit for Microsoft Excel. Berkeley Geochronology Center. Special Publication No. 4, pp. 1–67.
Luo, Y., Sun, M., Zhao, G.C., Li, S.Z., Xu, P., Ye, K., Xia, X.P., 2004. LA-ICP-MS U–Pb zircon ages of the Liaohe Group in the Eastern Block of the North China Craton: constraints on the evolution of the Jiao-Liao-Ji Belt. Precambrian Research 134, 349–371.
Lustrino, M., 2005. How the delamination and detachment of lower crust can influence basaltic magmatism. Earth-Science Reviews 72, 21–38.
Lu, S.N., Zhao, G.C., Wang, H.C., Hao, G.J., 2008. Precambrian metamorphic basement and sedimentary cover of the North China Craton: Review. Precambrian Research 160, 77–93.

Ma, X.Y., Suo, S.T., Wen, L.F., Wang, W.X., 1975. Paleostructural type of the Sinian System, Songshan area, Henan Province. Scientia Geologica Sinica (1), 12–31 (in Chinese).
Macpherson, C.G., Dreher, S., Thirlwall, M.F., 2006. Adakites without slab melting: high pressure differentiation of island arc magma, Mindanao, the Philippines. Earth and Planetary Science Letters 243, 581–593.
Martin, H., 1999. Adakitic magmas: modern analogues of Archaean granitoids. Lithos 46, 411–429.
Martin, H., Smithies, R.H., Rapp, R., Moyen, J.F., Champion, D., 2005. An overview of adakite, tonalite–trondhjemite–granodiorite (TTG), and sanukitoid: relationships and some implications for crustal evolution. Lithos 79, 1–24.
Moyen, J.-F., 2009. High Sr/Y and La/Yb ratios: the meaning of the "adakitic signature". Lithos 112, 556–574.
Polat, A., Herzberg, C., Münker, C., Rodgers, R., Kusky, T., Li, J.H., Fryer, B., Delaney, J., 2006. Geochemical and petrological evidence for a supra-subduction zone origin of Neoarchean (ca. 2.5 Ga) peridotites, Central Orogenic Belt, North China Craton. Geological Society of America Bulletin 118, 771–784.
Polat, A., Kusky, T.M., Li, J.H., Fryer, B., Kerrich, R., Patrick, K., 2005. Geochemistry of Neoarchean (ca. 2.55–2.50 Ga) volcanic and ophiolitic rocks in the Wutaishan Greenstone Belt, Central Orogenic Belt, North China Craton: implications for geodynamic setting and continental growth. Geological Society of America Bulletin 117, 1387–1399.
Qi, J.Y., 1992. Metamorphic rock series of Taihua Group and conditions for its formation in eastern Qinling. Scientia Geologica Sinica 27, 94–107 (in Chinese with English abstract).
Rapp, R.P., Shimizu, N., Norman, M.D., Applegate, G.S., 1999. Reaction between slab-derived melts and peridotite in the mantle wedge: experimental constraints at 3.8 GPa. Chemical Geology 160, 335–356.
Rudnick, R.L., Fountain, D.M., 1995. Nature and composition of the continental crust: a lower crustal perspective. Reviews of Geophysics 33, 267–309.
Shirey, S.B., Hanson, G.N., 1986. Mantle heterogeneity and crustal recycling in Archean granite-greenstone belts: evidence from Nd isotopes and trace elements in the Rainy Lake area, Superior Province, Ontario, Canada. Geochimica et Cosmochimica Acta 50, 2631–2651.
Sisson, T.W., 1994. Gornblende-melt trace-element partitioning measured by ion microprobe. Chemical Geology 117, 331–344.
Smithies, R.H., 2000. The Archaean tonalite–trondhjemite–granodiorite (TTG) series is not an analogue of Cenozoic adakite. Earth and Planetary Science Letters 182, 115–125.
Smithies, R.H., Champion, D.C., 2000. The Archaean high-Mg diorite suite: links to tonalite–trondhjemite–granodiorite magmatism and implications for early Archaean crustal growth. Journal of Petrology 41, 1653–1671.
Sun, S.-S., McDonough, W.F., 1989. Chemical and isotopic systematics of oceanic basalts: implications for mantle composition and processes. In: Saunders, A.D., Norry, M.J. (Eds.), Magmatism in the Ocean Basins. Geological Society Special Publications 42, pp. 313–345.
Tam, P.Y., Zhao, G.C., Liu, F.L., Zhou, X.W., Sun, M., Li, S.Z., 2011. SHRIMP U–Pb zircon ages of high-pressure mafic and pelitic granulites and associated rocks in the Jiaobei massif: constraints on the metamorphic ages of the Paleoproterozoic Jiao-Liao-Ji Belt in the North China Craton. Gondwana Research 19, 150–162.
Taylor, S.R., McLennan, S.M., 1985. The Continental Crust: Its Composition and Evolution. Blackwell, Oxford.
Wan, Y.S., Liu, D.Y., Wang, S.Y., Zhao, X., Dong, C.Y., Zhou, H.Y., Yin, X.Y., Yang, C.X., Gao, L.Z., 2009. Early Precambrian crustal evolution in the Dengfeng area, Henan province (eastern China): constraints from geochemistry and SHRIMP U–Pb zircon dating. Acta Geologica Sinica 83, 982–999 (in Chinese with English abstract).
Wan, Y.S., Wilde, S.A., Liu, D.Y., Yang, C.X., Song, B., Yin, X.Y., 2006. Further evidence for ~1.85 Ga metamorphism in the Central Zone of the North China Craton: SHRIMP U–Pb dating of zircon from metamorphic rocks in the Lushan area, Henan Province. Gondwana Research 9, 189–197.
Wang, F., Li, X.P., Chu, H., Zhao, G.C., 2011. Petrology and metamorphism of khondalites from Jining Complex in the North China Craton. International Geology Review 53, 212–229.
Wang, Q., Xu, J.F., Jian, P., Bao, Z.W., Zhao, Z.H., Li, C.F., Xiong, X.L., Ma, J.L., 2006. Petrogenesis of adakitic porphyries in an extensional tectonic setting, Dexing, South China: implications for the genesis of porphyry copper mineralization. Journal of Petrology 47, 119–144.
Wang, Z.J., Shen, Q.H., Wan, Y.S., 2004. SHRIMP U–Pb zircon geochronology of the Shipaihe "metadiorite mass" from Dengfeng county, Henan Province. Acta Geoscientica Sinica 25, 295–298 (in Chinese with English abstract).
Wiedenbeck, M., Alle, P., Corfu, F., Griffin, W.L., Meier, M., Oberli, F., Vonquadt, A., Roddick, J.C., Speigel, W., 1995. 3 natural zircon standards for U–Th–Pb, Lu–Hf, trace-element and Ree analyses. Geostandards Newsletter 19, 1–23.
Williams, I.S., 1998. U–Th–Pb geochronology by ion microprobe. In: Applications of microanalytical techniques to understanding mineralizing processes. Reviews in Economic Geology 7 (1998) 1–35.
Wu, F.Y., Yang, Y.H., Xie, L.W., Yang, J.H., Xu, P., 2006. Hf isotopic compositions of the standard zircons and baddeleyites used in U–Pb geochronology. Chemical Geology 234, 105–126.
Xia, X.P., Sun, M., Zhao, G.C., Wu, F.Y., Xu, P., Zhang, J.H., Luo, Y., 2006a. U–Pb and Hf isotopic study of detrital zircons from the Wulashan khondalites: constraints on the evolution of the Ordos Terrane, Western Block of the North China Craton. Earth and Planetary Science Letters 241, 581–593.
Xia, X.P., Sun, M., Zhao, G.C., Luo, Y., 2006b. LA-ICP-MS U–Pb geochronology of detrital zircons from the Jining Complex, North China Craton and its tectonic significance. Precambrian Research 144, 199–212.
Xia, X.P., Sun, M., Zhao, G.C., Wu, F.Y., Xu, P., Zhang, J.S., 2008. Paleoproterozoic crustal growth events in the Western Block of the North China Craton: evidence from detrital zircon Hf and whole rock Sr–Nd isotopes of the khondalites in the Jining Complex. American Journal of Science 308, 304–327.
Xie, L.W., Zhang, Y.B., Zhang, H.H., Sun, J.F., Wu, F.Y., 2008. In situ simultaneous determination of trace elements, U–Pb and Lu–Hf isotopes in zircon and baddeleyite. Chinese Science Bulletin 53, 1565–1573.
Xu, J.F., Shinjo, R., Defant, M.J., Wang, Q., Rapp, R.P., 2002. Origin of Mesozoic adakitic intrusive rocks in the Ningzhen area of East China: partial melting of delaminated lower continental crust? Geology 30, 1111–1114.
Xu, X.S., Griffin, W.L., Ma, X., O'Reilly, S.Y., He, Z.Y., Zhang, C.L., 2009. The Taihua group on the southern margin of the North China Craton: further insights from U–Pb ages and Hf isotope compositions of zircons. Mineralogy and Petrology 97, 43–59.
Yin, C.Q., Zhao, G.C., Guo, J.H., Sun, M., Xia, X.P., Zhou, X.W., Liu, C.H., 2011. U–Pb and Hf isotopic study of zircons of the Helanshan Complex: constrains on the evolution of the Khondalite Belt in the Western Block of the North China Craton. Lithos 122, 25–38.
Yin, C.Q., Zhao, G.C., Sun, M., Xia, X.P., Wei, C.J., Zhou, X.W., Leung, W.H., 2009. LA-ICP-MS U–Pb zircon ages of the Qianlishan Complex: constrains on the evolution of the Khondalite Belt in the Western Block of the North China Craton. Precambrian Research 174, 78–94.
Zegers, T.E., van Keken, P.E., 2001. Middle Archean continent formation by crustal delamination. Geology 29, 1083–1086.
Zhai, M.G., Bian, A.G., Zhao, T.P., 2000. The amalgamation of the supercontinent of North China Craton at the end of the Neoarchaean, and its break-up during the late Palaeoproterozoic and Mesoproterozoic. Science in China (D) 43 (Supplement), 219–232.
Zhai, M.G., Guo, J.H., Liu, W.J., 2005. Neoarchaean to Paleoproterozoic continental evolution and tectonic history of the North China Craton. Journal of Asian Earth Sciences 24, 547–561.
Zhai, M.G., Li, T.S., Peng, P., Hu, B., Liu, F., Zhang, Y.B., 2010. Precambrian key tectonic events and evolution of the North China Craton. In: Kusky, T.M., Zhai, M.G., Xiao, W. (Eds.), The Evolving Continents: Understanding Processes of Continental Growth. Special Publications, 338. Geological Society, London, pp. 235–262.
Zhang, G.W., Bai, Y.B., Song, Y., Guo, A.L., Zhou, D.W., Li, T.H., 1985. Composition and evolution of the Archean crust in central Henan, China. Precambrian Research 27, 7–35.
Zhang, J., Zhang, H.F., Lu, X.X., 2013. Zircon U–Pb and Lu–Hf isotope constraints on Precambrian evolution of continental crust in the Songshan area, the south-central North China Craton. Precambrian Research 226, 1–20.
Zhang, Z.Q., Li, S.M., 1988. Sm–Nd, Rb–Sr age and its geological significance of Archean Taihua Group in Xiongershan, western Henan Province. In: Chen, Y.Q. (Ed.), Contributions of Early Precambrian Geology in North China Craton. Geological Publishing House, Beijing, pp. 123–132 (in Chinese).
Zhao, G.C., 2001. Palaeoproterozoic assembly of the North China Craton. Geological Magazine 138, 87–91.
Zhao, G.C., 2009. Metamorphic evolution of major tectonic units in the basement of the North China Craton: key issues and discussion. Acta Petrologica Sinica 25, 1772–1792.
Zhao, G.C., Cawood, P.A., Li, S.Z., Wilde, S.A., Sun, M., Zhang, J., He, Y.H., Yin, C.Q., 2012. Amalgamation of the North China Craton: key issues and discussion. Precambrian Research 222, 55–76.
Zhao, G.C., Cawood, P.A., Wilde, S.A., Lu, L.Z., 2000. Metamorphism of basement rocks in the Central Zone of the North China Craton: implications for Paleoproterozoic tectonic evolution. Precambrian Research 103, 55–88.
Zhao, G.C., Cawood, P.A., Wilde, S.A., Sun, M., 2002b. Review of global 2.1–1.8 Ga orogens: implications for a pre-Rodinia supercontinent. Earth-Science Reviews 59, 125–162.
Zhao, G.C., Sun, M., Wilde, S.A., 2003a. Major tectonic units of the North China Craton and their Paleoproterozoic assembly. Science in China Series D: Earth Sciences 46, 23–38.
Zhao, G.C., Sun, M., Wilde, S.A., Li, S.Z., 2003b. Assembly, accretion and breakup of the Paleo-Mesoproterozoic Columbia Supercontinent: records in the North China Craton. Gondwana Research 6, 417–434.
Zhao, G.C., Sun, M., Wilde, S.A., Li, S.Z., 2004. A Paleo-Mesoproterozoic supercontinent: assembly, growth and breakup. Earth-Science Reviews 67, 91–123.
Zhao, G.C., Sun, M., Wilde, S.A., Li, S.Z., 2005. Late Archean to Paleoproterozoic evolution of the North China Craton: key issues revisited. Precambrian Research 136, 177–202.
Zhao, G.C., Wilde, S.A., Guo, J.H., Cawood, P.A., Sun, M., Li, X.P., 2010. Single zircon grains record two continental collisional events in the North China Craton. Precambrian Research 177, 266–276.
Zhao, G.C., Li, S.Z., Sun, M., Wilde, S.A., 2011. Assembly, accretion, and break-up of the Palaeo-Mesoproterozoic Columbia supercontinent: record in the North China Craton revisited. International Geology Review 53, 1331–1356.
Zhao, G.C., Wilde, S.A., Cawood, P.A., Sun, M., 2001. Archean blocks and their boundaries in the North China Craton: lithological geochemical, structural and P–T path constraints and tectonic evolution. Precambrian Research 107, 45–73.
Zhao, G.C., Wilde, S.A., Cawood, P.A., Sun, M., 2002a. SHRIMP U–Pb zircon ages of the Fuping complex: implications for Late Archean to Paleoproterozoic accretion and assembly of the North China Craton. American Journal of Science 302, 191–226.

Zhao, G.C., Wilde, S.A., Sun, M., Li, S.Z., Li, X.P., Zhang, J., 2008a. SHRIMP U–Pb zircon ages of granitoid rocks in the Lüliang complex: implications for the accretion and evolution of the Trans-North China Orogen. Precambrian Research 160, 213–226.

Zhao, G.C., Wilde, S.A., Sun, M., Guo, J.H., Kroner, A., Li, S.Z., Li, X.P., Wu, C.M., 2008b. SHRIMP U–Pb zircon geochronology of the Huai'an Complex: constraints on Late Archean to Paleoproterozoic crustal accretion and collision of the Trans-North China Orogen. American Journal of Science 308, 270–303.

Zhao, G.C., Zhai, M.G., 2013. Lithotectonic elements of Precambrian basement in the North China Craton: review and tectonic implications. Gondwana Research 23, 1207–1240.

Zhou, H.W., Zhong, Z.Q., Ling, W.L., Zhong, G.L., Xu, Q.D., 1998. Sm–Nd isochron for the amphibolites within Taihua Complex from XiaoQinling area, western Henan and its geological implications. Geochimica 27, 367–372 (in Chinese with English abstract).

Zhou, X.W., Zhao, G.C., Geng, Y.S., 2010. Helanshan high-pressure pelitic granulites: petrological evidence for collision event in the Western Block of the North China Craton. Acta Petrological Sinica 26, 2113–2121.

Zhou, X.W., Zhao, G.C., Wei, C.J., Geng, Y.S., Sun, M., 2008. Metamorphic evolution and Th–U–Pb zircon and monazite geochronology of high-pressure pelitic granulites in the Jiaobei massif of the North China Craton. American Journal of Science 308, 328–350.

Zhou, Y.Y., Zhao, T.P., Wang, C.Y., Hu, G.H., 2011. Geochronology and geochemistry of 2.5 to 2.4 Ga granitic plutons from the southern margin of the North China Craton: implications for a tectonic transition from arc to post-collisional setting. Gondwana Research 20, 171–183.

Zhou, Y.Y., Zhao, T.P., Xue, L.W., Wang, S.Y., Gao, J.F., 2009. Petrological, geochemical and chronological constraints for the origin and geological significance of Neoarchean TTG gneiss in the Songshan area, North China Craton. Acta Petrologica Sinica 25, 331–347 (in Chinese with English abstract).